APPLICATION OF OPTIMAL FILTERING FOR STREAMFLOW FORECASTING

VINAY KANTAMNENI

Bachelor of Engineering in Electronics and Controls Engineering

Jawaharlal Nehru Technological University, India

APRIL 2003

Submitted in partial fulfillment of requirements for the degree

MASTER OF SCIENCE IN ELECTRICAL ENGINEERING

at the

CLEVELAND STATE UNIVERSITY

APRIL 2006

APPLICATION OF OPTIMAL FILTERING FOR STREAMFLOW FORECASTING

VINAY KANTAMNENI

ABSTRACT

This thesis describes the development of a streamflow forecasting model based on the Sacramento Soil Moisture Accounting Model and applies optimal filtering techniques to sequentially update watershed-scale soil moisture state values, to improve streamflow predictions. In general hydrology is the study of the waters of the earth, especially with relation to the effects of precipitation and evaporation upon the occurrence and character of water in streams, lakes and water on or below the land surface. The Sacramento soil moisture accounting model is a hydrologic simulation model developed by the National Weather Service, and used throughout the nation for operational streamflow forecasting. In continuous hydrologic simulation, the accumulation and propagation of errors in estimated values of the model states can degrade the quality of streamflow predictions. This research explores the use of robust filtering techniques to improve streamflow forecasting through state updating of the National Weather Service's Sacramento Soil Moisture Accounting model. Kalman and H-infinity filters are used to update daily estimates of the water content in model states representing watershed-scale soil moisture storage. Updated soil moisture storages are then used to predict daily streamflow. The output from the estimators is then compared with the model output without state updating, the simulation results from the National Weather Service and the observed streamflow. It is seen in this thesis that Kalman and H-infinity filtering provide improved streamflow forecasting compared with existing methods.

ACKNOWLEDGEMENT

I would like to express my sincere indebtness and gratitude to my thesis advisor Dr. Dan Simon, for the ingenious commitment, encouragement and highly valuable advice he provided me over the entire course of this thesis. I would like to thank Dr. Stuart Schwartz, Director of the Center for Environmental Science, Technology and Policy at Cleveland State University, for his support and constant guidance in the work. I would also like to thank my committee members Dr. Fuqin Xiong and Dr. Sridhar Ungarala for their support and advice. I wish to thank my lab mates at the Embedded Control Systems Research Laboratory for their encouragement and intellectual input during the entire course of this thesis without which this work wouldn't have been possible. Finally, I wish to thank my roommates and all my friends who have always been a constant source of inspiration to me.

TABLE OF CONTENTS

LIST OF FIGURES

LIST OF TABLES

CHAPTER I

INTRODUCTION

Rainfall runoff models are basically lumped parameter, continuous and conceptual models [12]. These models are called lumped because they aggregate temporal and spatial variability into average state variables. These are continuous as the state variables, which are antecedent conditions, are continuously updated, and therefore they have memory, which affects the system response at any time. These are conceptual states, which means we are representing abstractions of the dominant processes, not specific physical representations of processes active at any point in time or space.

Until the1960s most of the model studies addressed single events. There are many hydrologic simulation models like unit hydrograph [1], storm response models of Nash and Dooge [2], HEC-1 [3], and Storm Water Management Model (SWMM) [4]. Most of these models are not concerned with the time continuous estimation of the flow, but are concerned primarily with runoff volume and peak discharge. One of the most

significant conceptual time continuous, spatially lumped model is Stanford Watershed Model [5]. It produces a daily flow estimate from daily rainfall. The continuous development of this model has resulted in the Hydrologic Simulation Program [6]. Another version of the Stanford Watershed Model was developed by the Hydrologic Research Laboratory of National Weather Service [7]. A large number of conceptual lumped models have been developed during the 1960's and 1970's; some interesting ones are described in [8, 9, 10]. The model that is used in this thesis is the Sacramento soil moisture accounting model [19].

The Sacramento soil moisture accounting model is a lumped parameter, continuous conceptual model which is divided into six conceptual soil moisture states, two inputs and one output. Streamflow is computed by the Sacramento catchment model as the result of processing precipitation through an algorithm representing the uppermost soil mantle identified as the upper zone, and a deeper portion of the soil mantle or lower zone. The model utilizes a set of conceptual soil moisture storages of determinable capacities, which allow the system to approximate many of the soil moisture conditions that control the production of streamflow. The storages are filled if sufficient rain occurs, and their contents are depleted by vertical percolation, evapotranspiration, and lateral drainage.

The inputs of the system are derived from meteorological measurements, from which streamflow is calculated. The results that are obtained from calculation are then compared with the known values of the flow. In order to predict the streamflow, a known set of data of inputs and the outputs from previous records are taken and then the model is initially calibrated to simulate the observed flow. The results that are obtained from calculation have errors in it. These errors are due to measurement error, model errors,

calibration errors, aggregation of errors over time, and errors in the input. In order to make the model more accurate by better prediction, optimal filtering techniques are used in this thesis.

The aim of this thesis is to implement optimal filtering techniques for the state space form of Sacramento soil accounting model [12]. Here Kalman filtering [29] and H-infinity filtering [31] are used and compared.

In order to understand how the filtering techniques can be useful for streamflow forecasting, we need to understand hydrology and the Sacramento soil accounting model. Chapter 2 discusses hydrology and explains the two different Sacramento soil accounting models: the Sacramento soil moisture accounting model (SAC-SMA) [19] and the state space form of Sacramento soil moisture accounting model first formulated by Kitanidis and Bras [14]. While the former model is widely used by the National Weather Service, the latter model is the state space form of the Sacramento soil accounting model, which has a number of approximations and simplifying assumptions that are documented and explained in [14]. The Sacramento soil moisture accounting model was re-cast in state space form (SS-SAC-SMA), specifically to make it possible to apply the Kalman filter for state updating.

The Sacramento soil moisture accounting model calibration, implementation of channel routing model and snowmelt model are discussed in Chapter 3. The Sacramento soil moisture accounting model is associated with errors in measurement, model errors, calibration errors, aggregation of errors over time, and errors in the input. In order to overcome the errors optimal filtering techniques are used. Here Kalman filtering [29] and

H-infinity filtering [31] are used. The details of the Kalman filter and H-infinity filter are described in Chapter 4.

The results of this thesis are comparisons of the simulations that are obtained by the National Weather Service, and by the Kalman and H-infinity filters with observed daily streamflow at the USGS stream gauge for the Deer Creek watershed at Mt. Sterling are discussed in Chapter 5. Conclusions and future work are described in Chapter 6.

CHAPTER II

HYDROLOGY AND THE SACRAMENTO SOIL MOISTURE ACCOUNTING MODEL

The Sacramento Soil Moisture Accounting Model (SAC-SMA) [19] is the spatially lumped parameter, continuous hydrologic simulation model used by the National Weather Service (NWS) for river forecasting at the nation's River Forecast Centers (RFCs). The Sacramento model simulates the rainfall runoff processes of the land phase of the hydrologic cycle. The model is referred to as a soil moisture accounting model because it simulates the mass balance through which precipitation is partitioned among evapotranspiration, infiltration, runoff, and soil moisture storage. The model is referred to as a continuous soil moisture accounting model, because the mass balance simulation of the rainfall runoff process is updated on regular (in this thesis daily) time intervals, maintaining a current estimate of watershed-scale soil moisture as the antecedent conditions to predict streamflow.

This chapter deals with the following topics required to develop a flow forecasting system:

1. Hydrology
2. The Sacramento model
3. Snowmelt models
4. Routing models

Section 2.1 gives an overview of the elements of hydrology. Section 2.2 discusses how the Sacramento model is formulated, and presents its mathematical equations. Section 2.3 discusses the implementation of a snowmelt model. Section 2.4 deals with the formulation of a hydrologic routing model, and Section 2.5 gives a brief overview of the catchment on which the Sacramento model is implemented.

2.1 Hydrology

Hydrology is the study of the waters of the earth, especially in relation to the effects of precipitation and evaporation on the occurrence and character of water in streams and lakes, and water on or below the land surface. Figure 2.1 gives a basic depiction of the hydrologic cycle.

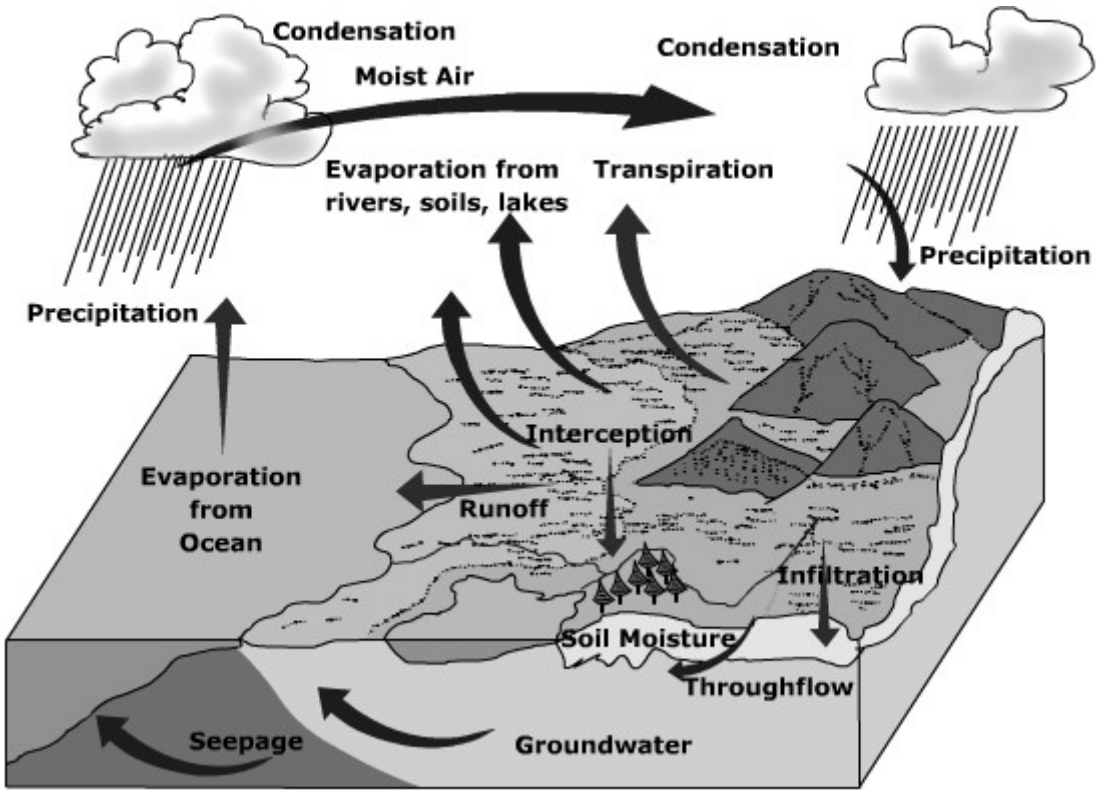

Figure 2.1: Basic hydrologic cycle [17].

2.1.1 Precipitation

Precipitation [11] can be of many types. Meteorologists commonly distinguish rainfall as convective or stratiform precipitation. Complex weather systems including extratropical cyclones, thunderstorms, and orographic precipitation generally consist of a mixture of both stratiform and convective precipitation [11]. It is basically classified according to the conditions that generate vertical air motion. Convectional precipitation is the normal precipitation that occurs in the Continent, especially in summer. Orographic precipitation results from the mechanical lifting of moist horizontal air currents over natural barriers such as mountain ranges. Cyclonic precipitation is associated with the movement and lifting of air masses from high pressure to low-pressure regions. Precipitation varies geographically, temporally and seasonally. Total precipitation is

distributed in numerous ways and when intercepted by vegetation and trees, may be equivalent to the total precipitation for relatively small storms. Once interception storage is filled, raindrops begin to fall from leaves and grass, where water stored on these surfaces eventually becomes depleted through evaporation. Precipitation reaches the ground in several ways. Some water fills depressions in impervious surfaces and eventually evaporates, and some water infiltrates the soil. The main losses from precipitation include interception, evaporation, depression storage and infiltration. These are defined as "losses" in the sense that they are not available to produce surface runoff.

2.1.2 The Basic Water Balance Equation

Runoff = Rainfall – Evapotranspiration – Changes in soil moisture.

From the above equation it can be said that the rainfall in a catchment is utilized either by vegetation, evaporation, changes in soil moisture storage or runoff.

2.1.3 Evapotranspiration

Evapotranspiration is the water returned to the atmosphere by two processes – evaporation and transpiration. Evaporation is the loss from open bodies of water, such as lakes and reservoirs, wetlands, bare soil, and snow cover; transpiration is the loss from living plant tissues to air [11]. Factors other than the physical characteristics of the water, soil, snow, and plant surface also affect the evapotranspiration process. The more important factors include net solar radiation, surface area of open bodies of water, wind speed, density and type of vegetative cover, availability of soil moisture, root depth, reflective land-surface characteristics, and season of year. Evapotranspiration is

dependent primarily on the solar energy available to vaporize the water. Because of the importance of solar energy, evapotranspiration also varies with latitude, season of year, time of day, and cloud cover.

Another important climatic factor that contributes to evapotranspiration is wind speed. Winds affect evapotranspiration by bringing heat energy into an area and removing the vaporized moisture. For example, a 5-mile-per-hour wind increases still-air evapotranspiration by 20 percent relative to no wind; a 15-mile-per-hour wind increases still-air evapotranspiration by 50 percent [12].

2.1.4 Soil Moisture

Water is diffused in the soil. Water is found in the upper part of the zone of aeration [11] from which it is returned to the atmosphere as water vapor by transpiration from plants or by soil evaporation. Soil water also drains into streams as base flow. There are three basic types of soil moisture, which can potentially influence catchment runoff conditions.

1. **Hygroscopic water**: Hygroscopic water is found as a microscopic film of water surrounding soil particles. This water is tightly bound to a soil particle by molecular forces so powerful that it is difficult for natural forces to remove it [11]. Hygroscopic water is bound to soil particles by adhesive forces that exceed 31 bars and may be as great as 10,000 bars [11]. (Recall that sea level pressure is equal to 1013.2 millibars, which is just about 1 bar.) The magnitude of hygroscopic soil moisture change is not only a function of soil type and lower level soil moisture, but also a function of dew point or

temperature at which atmospheric moisture condenses. Hygroscopic moisture does not influence the streamflow.

2. **Tension water**: Tension water refers to the water that is held between soil particles against the force of gravity. This water can be separated from the soil and returned to the atmosphere through the normal evapotranspiration process. Cohesive forces between the films of hygroscopic water hold tension water. The binding pressure for tension water is much less than hygroscopic water. This water can be removed by air drying or by plant absorption, but cannot be removed by gravity. Plants extract this water through their roots until the soil capillary force (force holding water to the particle) is equal to the extractive force of the plant root. Beyond this point, the plant cannot pull water from the plant-rooting zone; therefore, it wilts (called the wilting point). The actual volume of tension water within the soil is determined by an interrelationship between the area's climate, the catchment's soil types, and the characteristics of the plant forms, which exists in the catchment.

3. **Free water**: Free water is water that drains by the force of gravity. The amount of water held in the soil after excess water has drained is called the field capacity of the soil. The field capacity of water in the soil is controlled by the soil texture and the soil structure. Soils dominated by clay-sized particles have more total pore space in a unit volume than soils dominated by sand. As a result, fine-grained soils may have higher field capacities than coarse-grained soils. When soil particles in the zone, are deficient with tension water, those particles which are tension water deficient absorb free water to fulfill its tension water requirement.

The relative components of hygroscopic, tension and free water, which can be held within the soil, vary with soil types, soil structure, and organic content.

2.1.5 Interception

When rainfall occurs, a portion of the falling precipitation may remain suspended above the soil surface until trees and other vegetation, which can intercept precipitation, are sufficiently wet so that additional rainfall is transferred to the ground surface. This volume of water that is prevented from reaching the soil surface is called the intercepted water.

2.2 Sacramento Soil Moisture Accounting Model

The Sacramento soil moisture accounting model was developed by Burnash et al. in 1973 [19] to forecast the river flow in the California-Nevada region where the antecedent approach was deficient.

The Sacramento soil moisture accounting model is a lumped parameter, continuous, conceptual hydrologic model which is divided into six conceptual soil moisture states and two inputs and one output. Streamflow is computed by the Sacramento catchment model as the result of processing precipitation through an algorithm representing the uppermost soil mantle identified as the upper zone and a deeper portion of the soil mantle or lower zone. The model utilizes a set of conceptual soil moisture storages of determinable capacities, which allow the system to approximate many of the soil moisture conditions that control the production of streamflow. The storages are filled if sufficient rain should

occur, and their contents are depleted by vertical percolation, evaporation and lateral drainage.

The streamflow forecasting model has two inputs to the system: mean areal precipitation and potential evapotranspiration (Here potential evapotranspiration, which can be estimated from pan evapotranspiration is different from actual evapotranspiration. Potential evapotranspiration is the maximum evapotranspiration demand that can be satisfied. Here the factors affecting the evapotranspiration that are discussed in the previous section are not taken into consideration. Actual evapotranspiration in a given area is less than potential evapotranspiration.). The six soil moisture states of the Sacramento soil moisture accounting model are upper zone tension water, upper zone free water, lower zone tension water, lower zone free water primary, lower zone free water secondary and additional impervious water. The output of the system is streamflow. Estimated time series of mean areal precipitation and potential evapotranspiration are the two input time series from which the streamflow is simulated. The Sacramento soil moisture accounting model is continuous; based on the inputs the states are updated and output is calculated. The simulated streamflow provides an estimate of streamflow observed at the watershed outlet.

In order to predict streamflow a historical streamflow and meteorological data are used to calibrate the model, calibration is discussed in the next chapter. The model simulated results have errors [13] including measurement errors, model errors, calibration errors, aggregation of errors and errors in the input and the output. In order to make the system more accurate, filtering techniques [13, 20] can be used to update states, and then these updated states are used to calculate an updated forecast of the streamflow. Figure

2.2 shows the basic structure of the conceptual Sacramento soil moisture accounting model and its procedures.

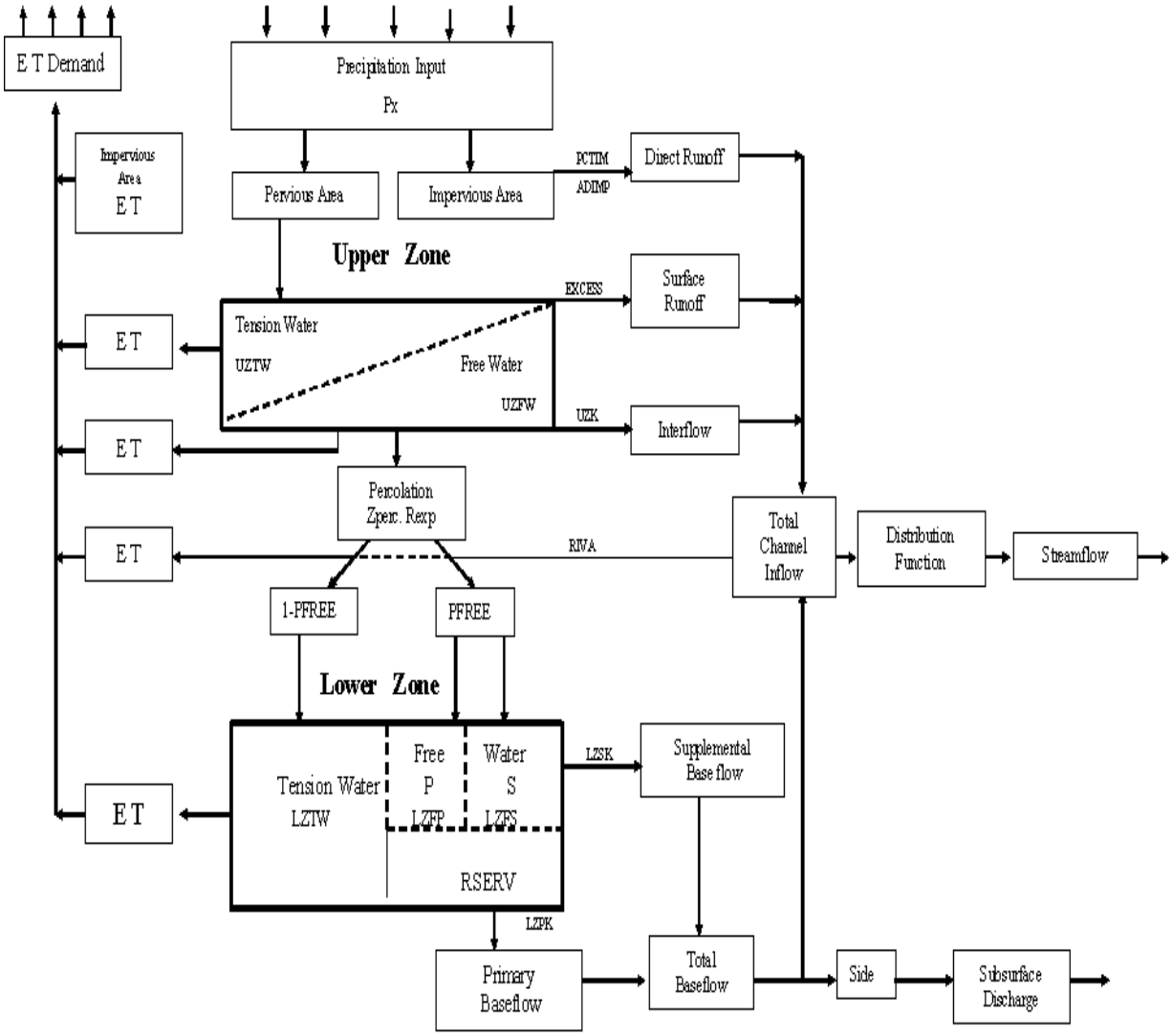

Figure 2.2: The structure of the Sacramento catchment model [18].

2.2.1 Principle of Waterflow in Sacramento Soil Moisture Accounting Model

When rainfall occurs over a catchment, precipitation, which falls over the impervious areas such as rocks, hard soil, ponds, lakes, and streams, generates direct runoff. The remaining precipitation falls on pervious areas where most of the precipitation may infiltrate into the soil.

The Sacramento soil moisture accounting model divides the soil into two zones, namely:

1. Upper zone
2. Lower zone

This upper zone in the model is modeled as two conceptual soil moisture states (reservoirs), namely:

1. Upper zone tension water
2. Upper zone free water

The lower zone is again divided into three soil moisture contents, namely:

1. Lower zone tension water
2. Lower zone free water
    a. Supplementary free water storage
    b. Primary free water storage

When water gets into the upper zone the water is absorbed by the upper zone soil and held as tension water, if tension water is deficient. When the upper zone tension water requirements are met, i.e., when there is sufficient upper zone tension water, the water is free to flow within the surface. This is called upper zone free water. Percolation, the rate of vertical drainage to deeper soils, is controlled by the content of the upper zone free

water and the deficiency of lower zone moisture volumes [19]. The preferred path for moisture in upper zone free water is considered to be downward as percolation. Horizontal flow in the form of interflow occurs only when the rate of precipitation exceeds the rate at which percolation can occur from the upper zone free water. When the precipitation rate exceeds both the percolation rate and the maximum interflow drainage capacity, then the upper zone free water capacity will be completely filled and the excess precipitation will result in surface runoff. Percolation, the transfer of water from upper soil to the lower soil, supplies moisture to three lower storage zones. The water is percolated from upper zone to lower zone where the water is absorbed by the lower zone for its tension water requirements. Then this water is allowed to drain by gravity, which in turn increases the lower zone primary and secondary free water storages.

Free water storages fill simultaneously from percolated water and drain independently at different rates, producing a variable ground water recession. Lower zone free water contributes to the base flow in that catchment. The base flow in the catchment is maximum when both the lower zone free water storages are at their maximum capacities. When the soil moisture requirements are met, the excess rainfall constitutes to surface runoff and direct runoff.

Streamflow is computed by the Sacramento catchment model as the result of processing precipitation through an algorithm representing the uppermost soil mantle as the upper zone and a deeper portion of the soil mantle or lower layer. Figure 2.3 shows the working model of Sacramento catchment model.

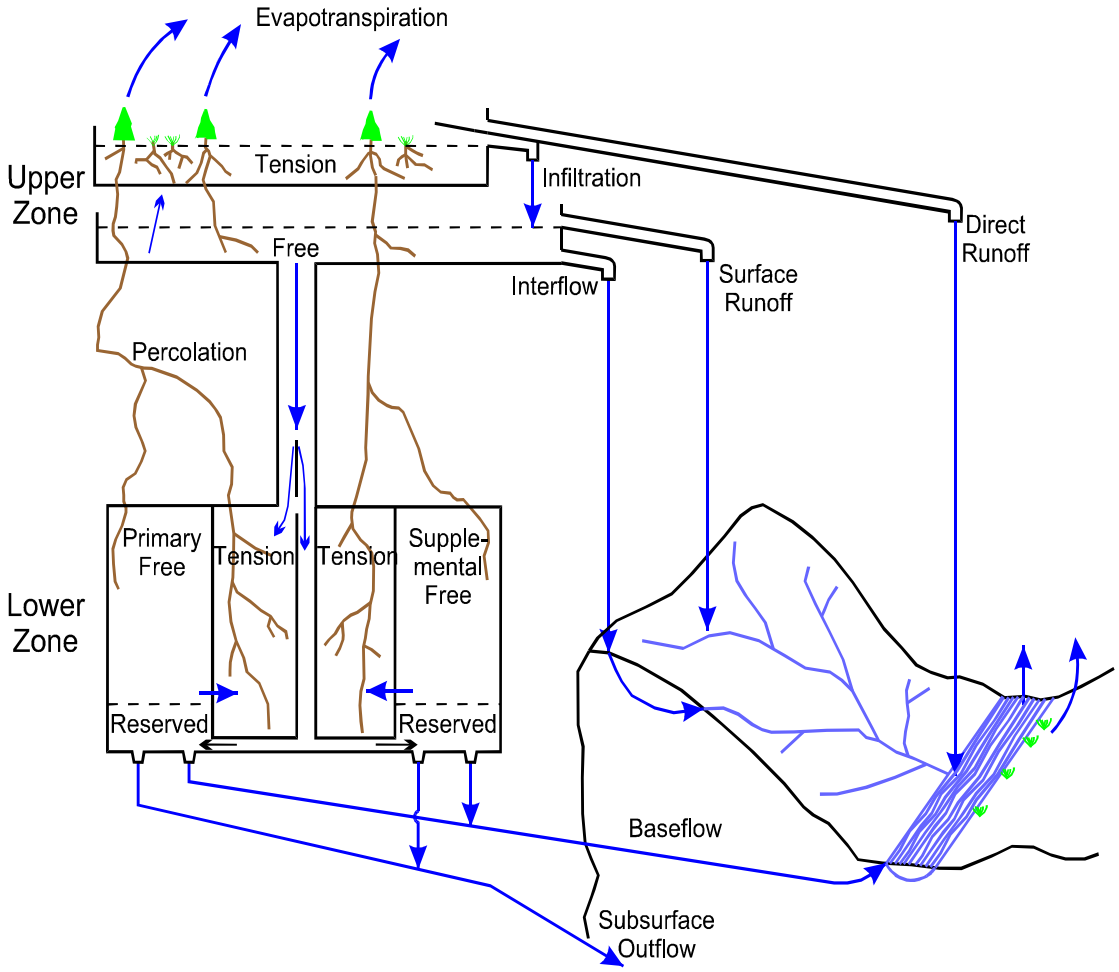

Figure 2.3: Working model of Sacramento catchment model [18].

2.2.2 Five Basic Waterflows

The five water flows computed by the Sacramento model are as follows:

1. Direct runoff from permanent and temporary impervious areas.

2. Surface runoff due to precipitation occurring at a rate faster than percolation, and interflow can take place when both upper zone storages are full.

3. Interflow resulting from the lateral drainage of free water storage.

4. Supplemental base flow.
5. Primary base flow.

The model utilizes a set of storages of determinable capacities, which allow the system to approximate many of the soil moisture conditions that in turn control the production of streamflow. The storages are filled if sufficient rain occurs, and their contents depleted by vertical percolation, evaporation, and lateral drainage.

2.2.3 Mathematical Calculations

This section discusses the mathematical calculations involved in the Sacramento soil moisture accounting model (SAC-SMA) [19] which is used by the National Weather Service for streamflow predictions, and the state space form of Sacramento soil moisture accounting model (SS-SAC-SMA) [12, 14] for which optimal filtering techniques are implemented. Sacramento soil moisture accounting model was re-cast in state space form to obtain state space form of Sacramento soil moisture accounting model, specifically to make it possible to apply the Kalman filter [29] for state updating. Given below are the mathematical calculations and variables involved in the Sacramento Soil moisture accounting model, which is used by the National Weather Service (NWS).

1. INTERFLOW = UZK * UZFWC

   UZK is the upper zone free water storage depletion coefficient and

   UZFWC is the volume of free water stored in the upper zone after immediate percolation requirements are met.

2. PBASE = ((LZFPM * LZPK) + (LZFSM * LZSK))

   PBASE is the percolation base rate.

LZFPM is the maximum storage capacity of those Lower Zone Free water primary.

LZPK is the depletion coefficient of Lower Zone Free water's primary storage.

LZFSM is the maximum storage capacity of those Lower Zone Free water secondary.

LZSK is the depletion coefficient of Lower Zone Free water's Supplementary storage.

3. MAXIMUM PERCOLATION RATE = PBASE*(1+Z)

4. $LZPD = PBASE\ (1 + Z*f\ (DEWET)^{REXP})$

LZPD is the Lower Zone percolation demand.

DEWET = 1 – (sum of lower zone contents) divided by (sum of lower zone capacities).

REXP is the degree of wetting.

Z is proportional increase in percolation.

5. $PERC = PBASE\ (1 + Z*f\ (DEWET)^{REXP})* UZFWC / UZFWM$

UZFWM is the maximum storage capacity of the Upper Zone Free water.

PERC is the percolation to lower zone.

6. Base flow= (VOLUME 1) * (DRAINAGE FACTOR)+(VOLUME 2)*(DRAINAGE FACTOR)

VOLUME 1 is primary storage = LZFWPC.

VOLUME 2 is secondary storage = LZFWSC.

7. $K = (Qpt/Qpo)^{1/t}$

K is daily recession coefficient of primary base flow.

t is the number of days.

Qpo is discharge when recession occurs at the primary rate.

Qpt is discharge t days after Qpo when the recession is continues at primary rate.

8. LZPK = 1 − K

9. LZFPM = QPMAX/LZPK

QPMAX is the maximum primary base flow.

10. PCITM is the increment of runoff produced by rainfall/the quantity of rainfall, which produced the runoff.

PCTIM is the fraction of catchment producing impervious runoff.

11. ADIMP = (EIA – PCTIM)/((TTC– IE)/TTC)

ADIMP is additional impervious area.

EIA is the effective impervious area.

TTC is the total tension water capacity.

IE is the intervening evapotranspiration during dry period.

The Sacramento model has been represented in state space form as a set of differential equations [12]. The state space representation of the Sacramento soil moisture accounting model makes a number of approximations and simplifying assumptions in order to represent the model in state space form [14]. This model can be written as a system having two inputs and six non-negative states. The state space formulation of the Sacramento model is developed in Kitanidis and Bras [14], and this model is further refined in Bae and Georgakakos [12]. Optimal filtering techniques are applied to the state space model.

The system states are defined as follows:

x_1 = upper zone tension water content

x_2 = upper zone free water content

x_3 = lower zone tension water content

x_4 = lower zone primary free water content

x_5 = lower zone secondary free water content

x_6 = additional impervious storage

The inputs of the system are given as follows:

U_p = mean areal precipitation

U_e = mean areal potential evapotranspiration demand

The differential equation for upper zone tension water element is given as:

$$\frac{dx_1}{dt} = \left[1 - \left(\frac{x_1}{x^o_1}\right)^{m1}\right] u_p - u_e \left(\frac{x_1}{x^o_1}\right)$$

The differential equation for upper zone free water element is given as:

$$\frac{dx_2}{dt} = \left(\frac{x_1}{x^o_1}\right)^{m1} u_p \left[1 - \left(\frac{x_2}{x^o_2}\right)^{m2}\right] - d_u x_2 - C_1(1+\varepsilon y^{\theta})\left(\frac{x_2}{x^o_2}\right)$$

The differential equation for lower zone tension water element is given as:

$$\frac{dx_3}{dt} = C_1(1+\varepsilon y^{\theta})\left(\frac{x_2}{x^o_2}\right)(1-p_f)\left[1 - \left(\frac{x_3}{x^o_3}\right)^{m3}\right] - u_e\left(1 - \frac{x_1}{x^o_1}\right)\left(\frac{x_3}{x^o_1 + x^o_3}\right)$$

The differential equation for lower zone primary water element is given as:

$$\frac{dx_4}{dt} = -d'_l x_4 + C_1(1+\varepsilon y^{\theta})\left(\frac{x_2}{x^o_2}\right)\left[1 - (1-p_f)\left[1 - \left(\frac{x_2}{x^o_2}\right)^{m3}\right]\right]\left[\left(C_2 \frac{x_5}{x^o_5} - 1\right)\left(\frac{x_2}{x^o_2}\right) + 1\right]$$

The differential equation for lower zone secondary water element is given as:

$$\frac{dx_5}{dt} = -d^{"}_{l} x_5 + C_1(1+\varepsilon y^{\theta})\left(\frac{x_2}{x^{o}_{2}}\right)\left[1-(1-p_f)\left[1-\left(\frac{x_3}{x^{o}_{4}}\right)^{m3}\right]\right]\left[(1-C_2\frac{x_5}{x^{o}_{5}})\left(\frac{x_4}{x^{o}_{4}}\right)\right]$$

The differential equation for additional impervious area water element is given as:

$$\frac{dx_6}{dt} = \left[1-\left(\frac{x_6}{x^{o}_{3}}\right)^{2}\left[1-\left(\frac{x_2}{x^{o}_{2}}\right)^{m2}\right]\left(\frac{x_1}{x^{o}_{1}}\right)^{m1}\right]u_p - u_e\left(1-\frac{x_1}{x^{o}_{1}}\right)\left(\frac{x_6}{x^{o}_{3}+x^{o}_{1}}\right)$$

The output u_c from the soil moisture accounting model, referred to as channel inflow per unit time, is given by:

$$u_c = \left(d_u x_2 + \frac{d^{"}_{l} x_4 + d_l^{"} x_5}{1+\mu}\right)(1-\beta_1-\beta_2) + u_p\beta_2 + \left(\frac{x_6}{x^{o}_{3}}\right)^{2} u_p\left(\frac{x_1}{x^{o}_{1}}\right)^{m1}\beta_1 +$$
$$u_p\left(\frac{x_1}{x^{o}_{1}}\right)^{m1}\left(\frac{x_2}{x^{o}_{2}}\right)^{m2}(1-\beta_1-\beta_2) + \left[1-\left(\frac{x_6}{x^{o}_{3}}\right)^{2}\right]\left(\frac{x_2}{x^{o}_{2}}\right)^{m2}\left(\frac{x_1}{x^{o}_{1}}\right)^{m1} u_p\beta_1$$

where

x^{o}_{1} is the upper zone tension water capacity .

x^{o}_{2} is the upper zone free water capacity.

x^{o}_{3} is the lower zone tension water capacity.

x^{o}_{4} is the lower zone primary free water capacity.

x^{o}_{5} is the lower zone secondary free water capacity.

d_u is the upper zone instantaneous drainage coefficient.

$d^{''}_{l}$ is the lower zone primary instantaneous drainage coefficient.

$d^{''}_{l}$ is the lower zone secondary instantaneous drainage coefficient.

C is the parameter in percolation function.

θ is the exponent in percolation function.

μ is the fraction of base flow not appearing in river flow.

β_1 is the fraction of basin that becomes impervious when tension water requirements are met.

β_2 is the fraction of basin presently impervious.

m_1 is the exponent of upper zone tension water nonlinear reservoir.

m_2 is the exponent of upper zone free water nonlinear reservoir.

m_3 is the exponent of lower zone tension water nonlinear reservoir.

2.3 Snowmelt Model

Snowmelt is also a factor for the channel flow in many northern catchment areas. In Ohio most of the snowmelt occurs in winter and early spring. In this region accurate estimates of snowmelt are important for streamflow forecasting.

Snowmelt occurs when the snowpack gains enough heat to induce the phase change from solid to liquid water. The main source of energy for snowmelt is solar radiation. In colder climates the accumulation and melting of snow can significantly influence the magnitude and timing in conversion of precipitation to runoff. Snow melts only when the heat content of snow rises above a certain threshold temperature. In order to simulate the snowmelt, a snowmelt model needs to be implemented.

Snowmelt can be computed by using different models but the most common ones are temperature index models [21] and energy balance models [22]. Temperature index models relate snowmelt to a simple index based on air temperature and empirical melt factors that vary with climate and land-use. Energy balance models are based on the physics of snowmelt and generally require a additional data that are often only partially available.

2.4 Channel Routing Model

The output of the Sacramento model is the average discharge of water from the soil to the streams over all the channels in the basin; it does not take into account the topography, the location, or the time it takes for the water to flow to the streams from land. It may take from a few hours to days for the water to move in the channel system to reach the watershed outlet. In order to consider this, a channel routing model is used. It is like a storage tank that stores the output of the Sacramento model and releases it slowly based on the time required to discharge. This is modeled as a set of linear reservoirs [12] where the outflow from one reservoir is led to the other reservoir.

Figure 2.4 gives an idealized representation of channel routing with a series of basic idea of how linear reservoirs work. As the outflow from one reservoir is the inflow to the other, the water that comes out of the channel routing model is delayed.

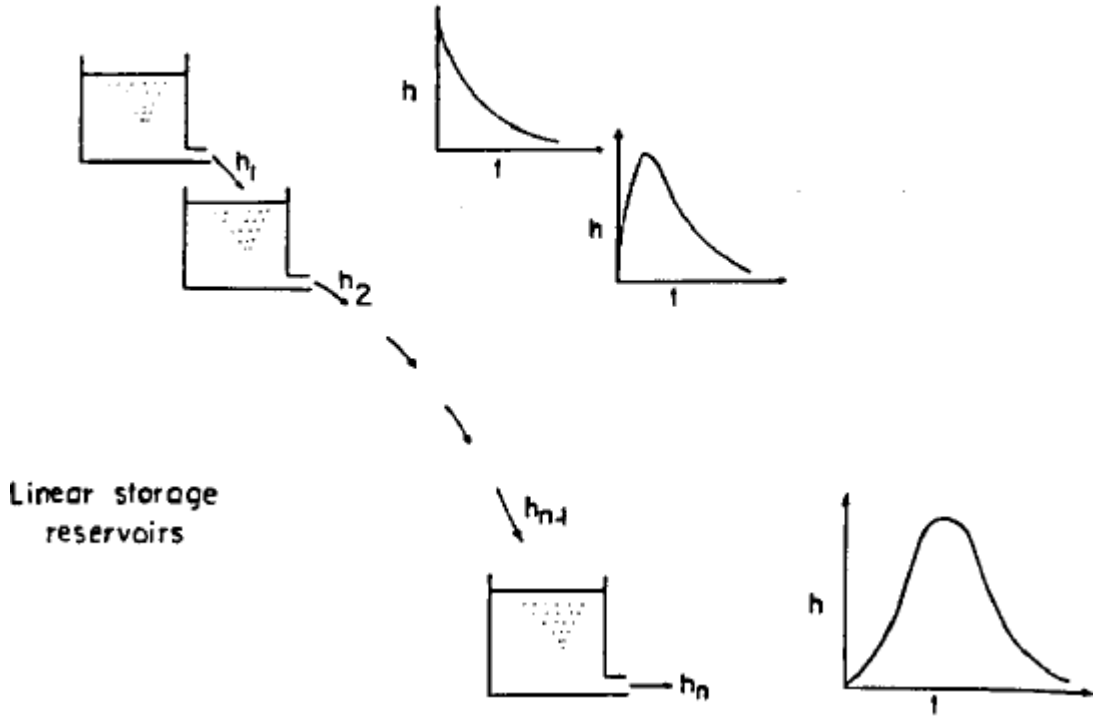

Figure 2.4: Cascade of linear reservoirs [23].

2.5 Problem Setting

The catchment that is used to implement the Sacramento model is located in the southwestern part of Ohio and it is called Deer Creek Basin, which is located in Madison County, Ohio. For river basin simulation, this basin is considered a headwater basin with no upstream watersheds and has no reservoirs, which makes it easy to calibrate. The basin is approximately 228 square miles in area, with a mean annual discharge of 200-300 cubic feet/sec. It has a maximum potential evapotranspiration of 5.7 inches in the month of July and a minimum of 0.30 inches in the month of January. The average monthly temperature is below 32^{o} F in the winter. Figure 2.5 shows the exact location of the Deer Creek watershed basin location.

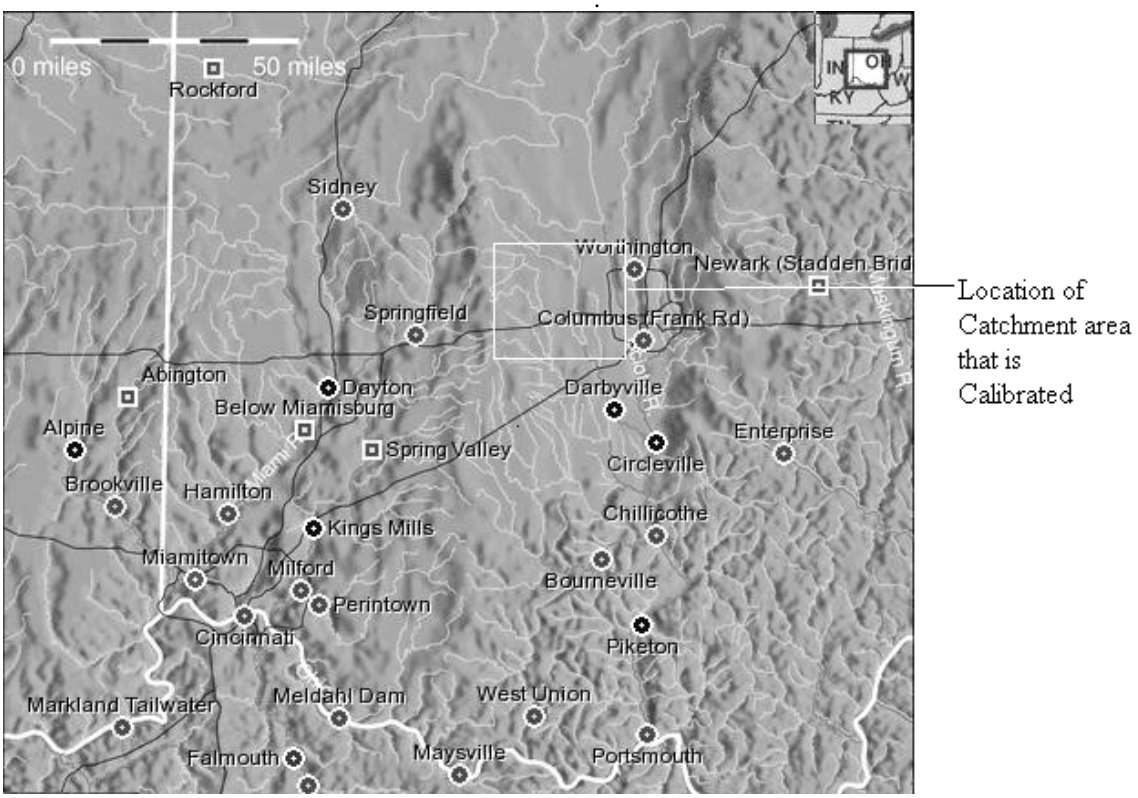

Figure 2.5: Location of Deer Creek watershed [18].

Streamflow from Deer Creek watershed for the period from 1966 to 1981 is recorded at the USGS stream gauge station number 03230800. Figure 2.6 shows the average monthly precipitation, observed flow and potential evaporation at the Deer Creek watershed. In this watershed, precipitation takes its maximum value in the spring with modest potential evapotranspiration (PET). This leads to highest levels of soil moisture and, with some streamflow. In spring and summer there is a modest decline of precipitation with minimum in summer, but very significant increase in PET as temperatures rise and vegetation blossoms. This results in declining soil moisture and minimum streamflow. As temperatures cool, evapotranspiration declines, plants become dormant, PET declines, precipitation gradually increases and soil moisture and streamflow recover in fall and winter, returning to maximum in spring. As winter temperatures in

Deer Creek watershed are frequently below freezing, snow and frozen precipitation are significant factor in the timing of runoff.

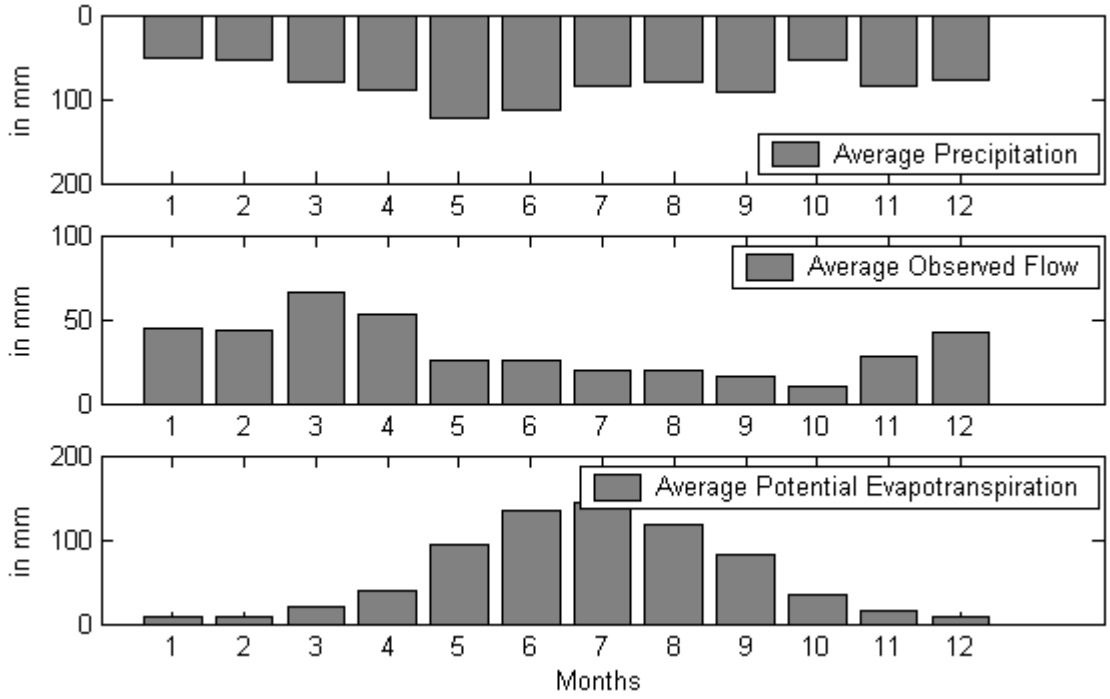

Figure 2.6: Monthly averages of precipitation, observed flow and potential evaporation.

The SAC-SMA is implemented by the NWS for the Deer Creek Watershed. As this model is continuous, lumped model, the errors in the internal states can accumulate. In operational forecasting, the model states are, periodically, manually adjusted to correct the cumulative error. The manual self adjust is done based on the experience of the hydrologist. In order to make the model autonomous, filtering techniques are used in this thesis. SAC-SMA was cast in state space form specifically to make it possible to apply Kalman filtering for state updating. In this thesis, H-infinity filtering is introduced for the SAC-SMA for the state updating and it is then compared with the Kalman filter.

CHAPTER III

CALIBRATION AND SIMULATION OF THE MODEL

Lumped parameter, continuous, conceptual hydrologic models are widely used in simulating catchment scale rainfall-runoff processes [12]. The parameters of these models cannot, in general, be determined directly from physical catchment characteristics, and hence the parameter values must be estimated by calibration against observed data.

This chapter describes parameter calibration and simulation. Section 3.1 gives details of basic guidelines for rainfall runoff model calibration. Section 3.2 discusses the calibration of Sacramento soil moisture accounting model and the detailed calibration for the Deer Creek Basin in Southwestern Ohio. Section 3.3 discusses the implementation of a channel routing model with the Sacramento soil moisture accounting model. Section 3.4 studies the effect of implementing a snowmelt model.

3.1 Calibration

Calibrating rainfall-runoff models involves consideration of the following objectives [24]:

1. A good agreement between the average observed and simulated catchment runoff volume (i.e., a good water balance).
2. A good agreement with the overall shape of the observed hydrograph.
3. A good agreement of peak flows.
4. A good agreement of low flows.

In the calibration process, the different calibration objectives (1)-(4) are taken into account. If the objectives are of equal importance, the hydrologist seeks to balance all the objectives. In the case of priority for a certain objective such as flood forecasting, one objective may be favored in the calibration process. In this respect it is important to realize that, in general, trade-offs exist between the different objectives. For instance, one may find a set of parameters that provide a very good simulation of high flows, but a poor simulation of low flows, and vice versa.

3.2 Sacramento Model Calibration

Initially the Sacramento soil moisture accounting model was calibrated without snowmelt model or channel routing. The Sacramento soil accounting model only represents the transformation of rainfall to runoff. As a conceptual model, the Sacramento soil moisture accounting model produces a conceptual total channel inflow, which is further modified through channel routing. The state space form of the Sacramento model

has 16 parameters [12], which are estimated and calibrated to replicate the observed streamflow. They are:

x^o_1 is upper zone tension water capacity .

x^o_2 is upper zone free water capacity.

x^o_3 is lower zone tension water capacity.

x^o_4 is lower zone primary free water capacity.

x^o_5 is lower zone secondary free water capacity .

d_u is upper zone instantaneous drainage coefficient.

d'_l is lower zone primary instantaneous drainage coefficient.

d''_l is lower zone secondary instantaneous drainage coefficient.

C is parameter in percolation function.

θ is exponent in percolation function.

μ is fraction of base flow not appearing in river flow.

β_1 is fraction of basin that becomes impervious when tension water requirements are met.

β_2 is fraction of basin presently impervious.

m_1 is exponent of upper zone tension water nonlinear reservoir.

m_2 is exponent of upper zone free water nonlinear reservoir.

m_3 is exponent of lower zone tension water nonlinear reservoir.

Here we incorporate human knowledge of the Sacramento model formulation [25] and calibration strategies into the calibration, where checks are difficult or impossible for a person to perform visually. This could help give physical meaning to model parameters, provide regional consistency in parameter sets, and help to avoid over-fitting of

parameters. Examples are enumerated below.

1. Use water balance approach to check the annual depth of storage required in the model.

2. Determine if the ratio of the upper and lower zone and tension and free water storage is reasonable. Lower zone is usually larger than upper, and lower zone free supplemental storage should be no more than half of the lower zone primary storage, etc. This may help prevent the over fitting of storage parameters for percolation or evapotranspiration losses.

3. Check range of contents of the storage reservoirs to ensure they're going through the appropriate cycles and have the appropriate range of storage. UZFW should fill on the largest events to generate surface runoff. One calibration strategy is to model fast response runoff with interflow by making the UZFWM large enough to hold large rain events and making UZK very large. This reduces the sensitivity of the Sacramento model to surface runoff triggering mechanisms and to over simulation due to precipitation errors. UZTW should always fill if observed runoff occurs, and should completely dry out during mid-length dry periods. LZTW should generally fill up to a maximum in the fall or winter and should probably nearly dry out during extended drought periods. LZFP should never dry out unless the stream is intermittent, and should generally fill during extended wet periods. LZFS should generally be empty, and only fill partially during intermediate runoff events, and possibly fill completely during large events in wet periods.

4. Perform “event analysis,” not time series analysis, where each runoff event is analyzed to determine if the appropriate Sacramento model components are working as

they generally should if parameterized correctly. For example, if it rains and observed runoff occurs, then tension water should fill too. Medium runoff events should probably be modeled with interflow. Large runoff events should probably have UZFW filled to generate surface runoff. However, some may choose to model fast response runoff by increasing UZK and UZFWM to reduce the sensitivity of surface runoff.

5. Check for data and modeling errors by analyzing inputs and outputs. If significant rain occurred and no runoff was observed, there may be a problem with the observed discharge data or rainfall data. Omit the resultant poor simulation section for the long-term statistical analysis. If there is observed runoff without rainfall, than there may be a problem with the rainfall data, particularly with convective events and gage networks, or snow events in the winter. Watch for missed rain/snow events in winter based on hydrograph response, temperature, or snow on ground data. If no snow model is used and snow is known to be present, then omit the winter months in output statistics.

All items listed in 1-5 above are the options that can be chosen to implement as needed. Here one should be able to make his/her own rules and set the guidelines so that they are appropriate for the hydrologic regime being modeled and they reflect local knowledge and calibration strategy being used. To estimate initial model parameters the initial calibration implemented the Sacramento soil moisture accounting model without snowmelt or channel routing. Initial model parameters were calibrated to reproduce the annual and monthly water balance. After getting a reasonable monthly water balance, the calibration is refined for individual storm simulation and extreme errors during dry and wet periods and calibrated. Then the simulated model is checked for persistent biases in under or over estimation and is calibrated. The timing of the peak flow and daily

discharge is considered and it is corrected with the channel routing model. After the model is able to closely reproduce the observed flow, the model simulation is checked in the early spring and in winter period to see the effects of the snowmelt. Upon comparing the simulation with actual observed data it is observed that there are events of streamflow which occurred when there is no precipitation and when there is a rise in temperature above 32^{o} F and vice versa. This implied that there is a need to model the snowmelt model as temperature changes strongly suggested snowmelt is affecting streamflow in the catchment area.

Based on these choices the calibration is done and the parameters are set to:

x^{o}_{1} upper zone tension water capacity = 22 mm

x^{o}_{2} upper zone free water capacity = 18 mm

x^{o}_{3} lower zone tension water capacity = 56 mm

x^{o}_{4} lower zone primary free water capacity = 65 mm

x^{o}_{5} lower zone secondary free water capacity = 17 mm

d_{u} upper zone instantaneous drainage coefficient = 0.7

d''_{l} lower zone primary instantaneous drainage coefficient = 0.003

d''_{l} lower zone secondary instantaneous drainage coefficient = 0.450

ϵ parameter in percolation function = 100

θ exponent in percolation function = 2.0

μ fraction of base flow not appearing in river flow = 0.2304

β_{1} fraction of basin that becomes impervious when tension water requirements are met = 0

β_{2} fraction of basin presently impervious = 0

m_1 exponent of upper zone tension water nonlinear reservoir = 2.1155

m_2 exponent of upper zone free water nonlinear reservoir = 1.7691

m_3 exponent of lower zone tension water nonlinear reservoir = 3.8873

The model is calibrated for a period of nine years starting from 1972 to 1980. Upon calibrating, the model is simulated and observed. The model when compared, responded well for a simulation period of nine years starting from 1967 to 1975. It was able to produce high flows, low flows and the all the layers in the Sacramento model had good response to the inputs. Figure 3.1 shows the simulation and precipitation from 1968 to 1970 without implementation of snowmelt or channel routing. The model depicted the high flows and the low flows. The low flows are observed between June and October and the high flows are observed between October and May of all the years.

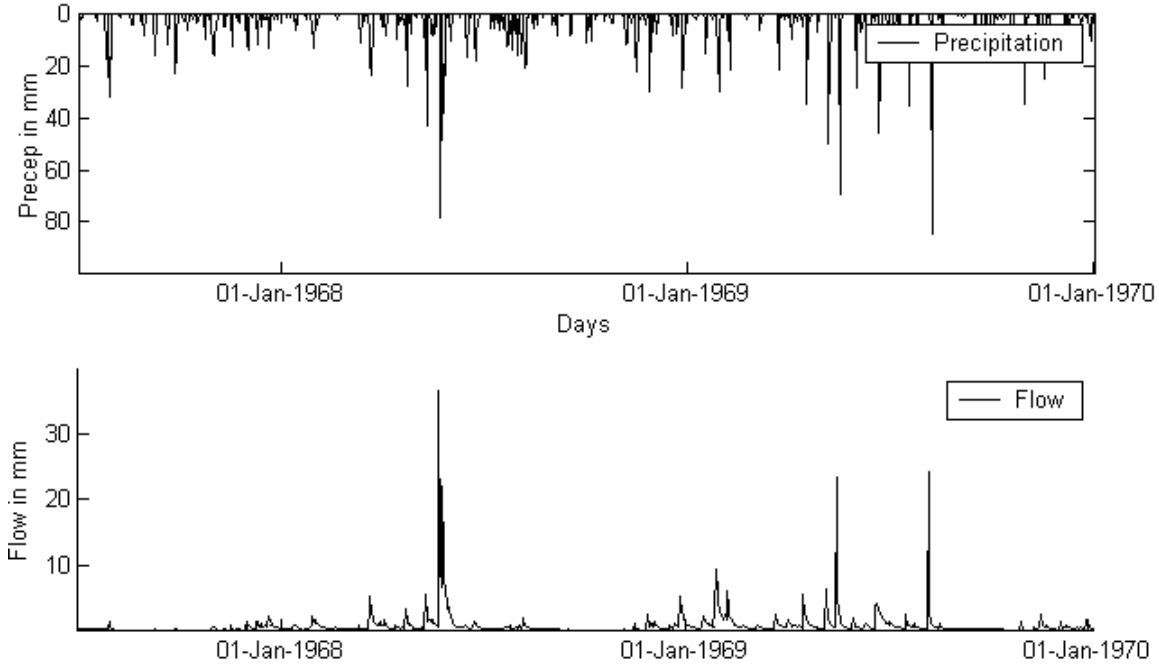

Figure 3.1: Precipitation and simulated Flow.

3.3 Channel Routing Model

The results obtained from the simulation without channel routing were then compared to the actual flow that was obtained from the US Geological Survey. Upon closer analysis the simulated peak flow occurs earlier than the observed flow peaks. Figure 3.2 shows the simulated flow verses the actual flow for a period of three months from Nov. 1967 to Jan. 1968. Here the simulated peaks are earlier than the observed flow. This is attributed to the lack of the channel routing in the model. The output of the Sacramento model is just the amount of discharge from the land surface to the stream channel network; it does not take into account the topography, location, or the time it takes for runoff to reach the stream outlet where the measurement is taken. It may take from a few hours to days for the water to discharge from the soil to the watershed outlet. In order to consider this, a channel routing model is used which is described in the previous chapter. This is like a storage tank mentioned in [12], which stores the output of the Sacramento model and releases it slowly based on the time required to discharge.

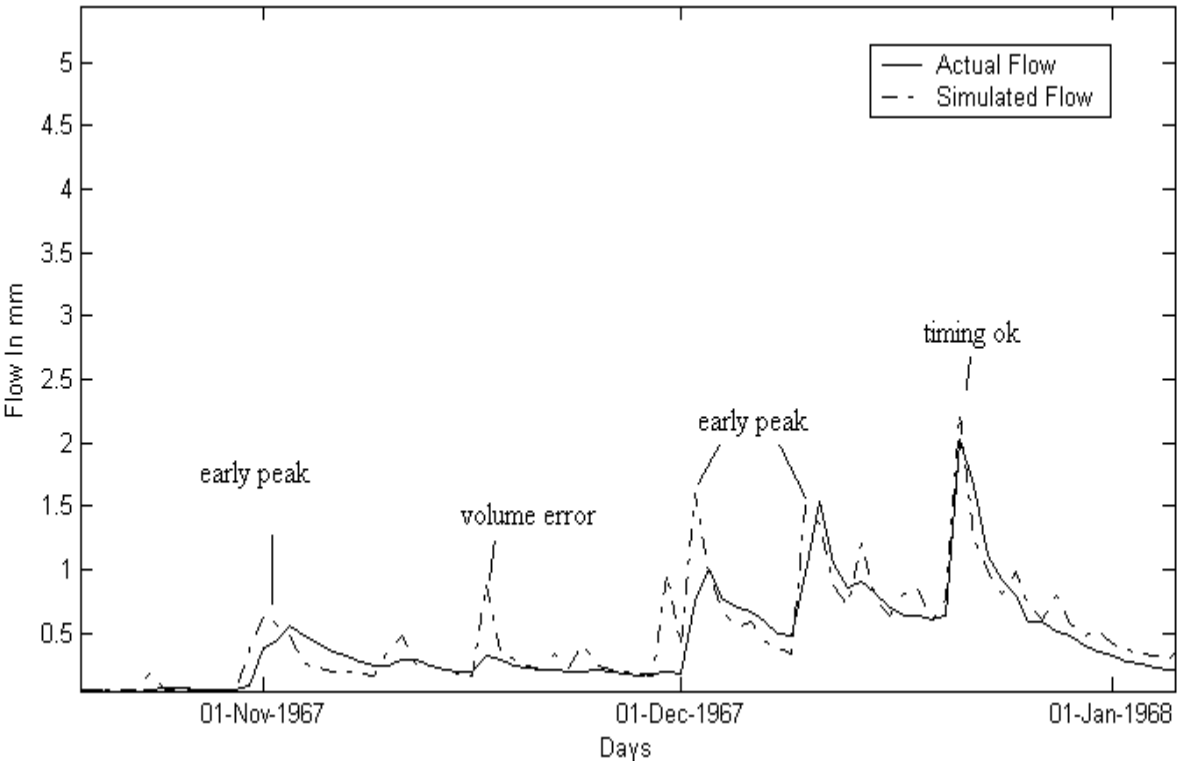

Figure 3.2: Actual flow and simulated flow.

The basic channel routing model [12] is selected and is implemented along with the Sacramento model code. The routing model equations are shown below. This model has two linear storage reservoirs s_1 and s_2 where water from s_1 flows into s_2 with a limiting factor α, where α is just a reservoir constant, which sets the linear drainage rate. The input to s_1 is the total channel inflow, i.e. Sacramento soil moisture accounting model output, the output of s_1 is input to s_2.

$$\dot{s}_1 = u_c - \alpha s_1$$
$$\dot{s}_2 = \alpha s_1 - \alpha s_2$$
$$f = \alpha s_2$$

where f is the routed flow.

Figure 3.3 shows the changes in daily average discharge timing with a unit (pulse) input with changes in the α value. Here the graphs are plotted for various values of α ranging from 5.25 to 20.25 for a unit input on a single day. When α is 5.25 the channel response extends more than seven days, but as the value of α is increased the response time decreases and channel response is more flashy. In this way increasing the value of α decreases the response time of the routing model.

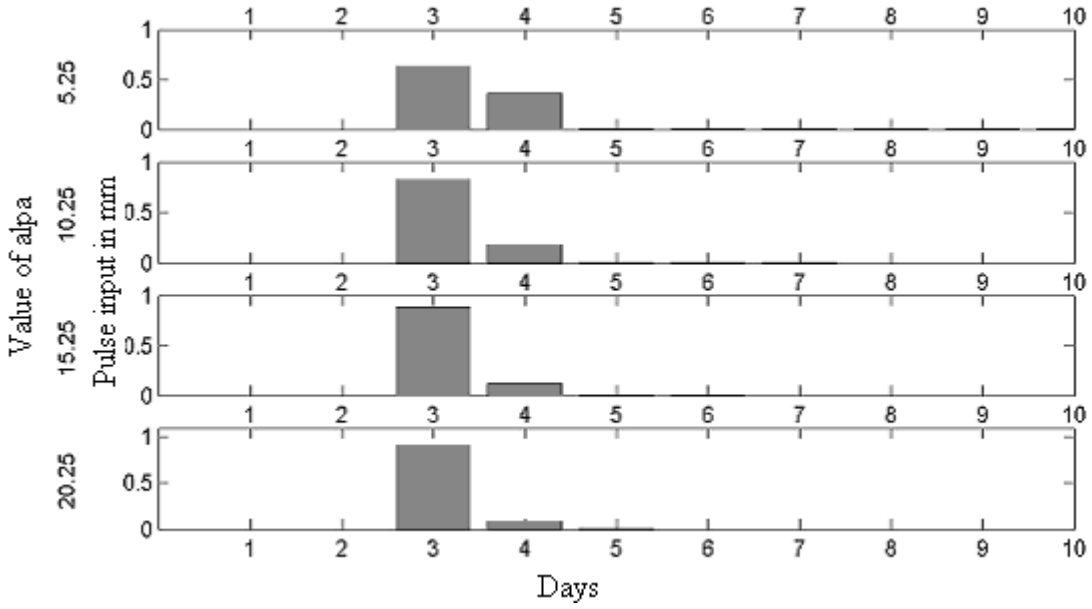

Figure 3.3: Values of α for a given pulse input.

The channel routing parameter is manually calibrated to a value of 22.5, thus resulting in a rapid response and improved timing and magnitude of the daily flow peaks. Upon implementing the channel routing model, the simulated flow is compared with the actual flow. Figure 3.4 shows the improvements that are obtained after implementing the channel routing model. The peaks of the simulated model are reduced and coincide more closely with the timing and magnitude of the actual flow.

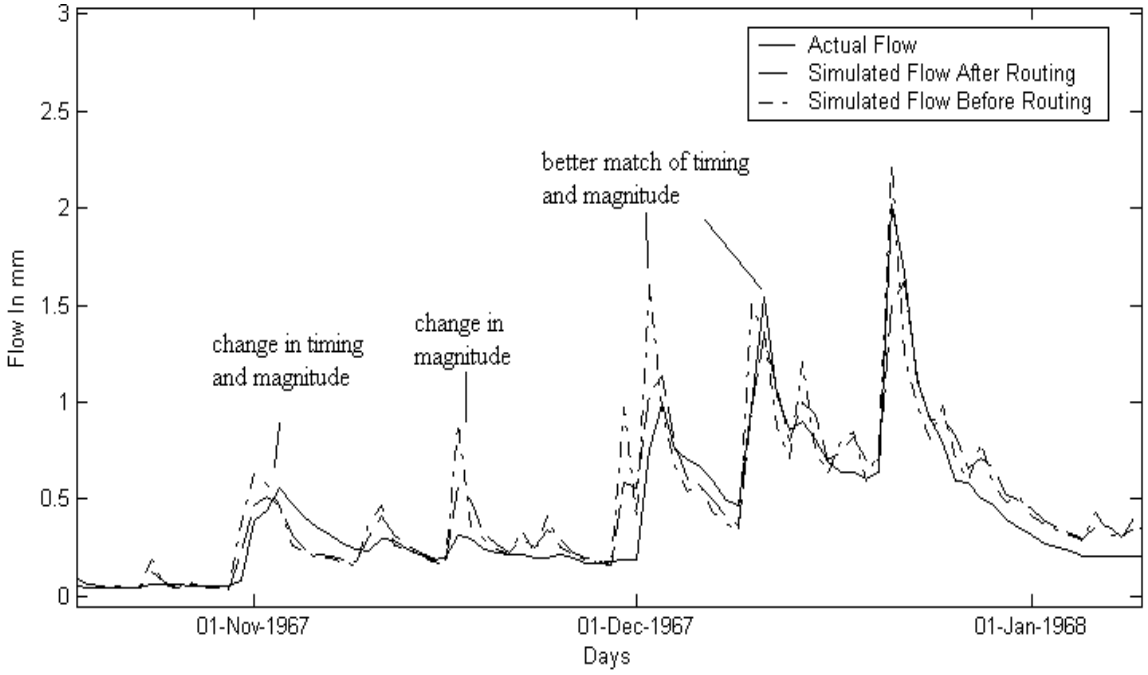

Figure 3.4: Flow comparison.

3.4 Snowmelt Model

Channel routing significantly improved daily and event based simulation of the peak flows. But upon closer observations of remaining daily simulated errors, the months from December to April, showed consistent simulation errors in peak timing and magnitude, when compared to the actual flow. Closer analysis revealed events, during which peak discharge occurred without precipitation, coinciding with a rise in temperature above 32^{o} F. Similarly observed precipitation events were observed that produced no significant runoff with temperature below freezing. The catchment area is located in the southwestern part of Ohio where snow accumulations does occur during winter. The NWS estimates snowmelt accounts for approximately 15% of the annual runoff. The consistent winter errors in peak runoff indicated the need to account for snow and snowmelt in simulating the rainfall runoff process for this watershed. Snowmelt

occurs as the snowpack gains heat. The main source of energy for snowmelt is solar radiation. Figure 3.5, illustrates simulation errors associated with freezing temperatures; when the temperature decreases below 32^{o} F, there is a consistent difference in the simulated and the observed flow. Here simulated flow is due to the precipitation, but the observed flow doesn't respond to that precipitation as the temperature is below 32^{o} F and so the precipitation is likely in the form of snow. Similarly in the month of March the simulation is over producing compared to the observed flow. On that particular day there is some precipitation that led to the simulated flow but the temperature is below 32^{o} F. The precipitation that occurred is interpreted as snow.

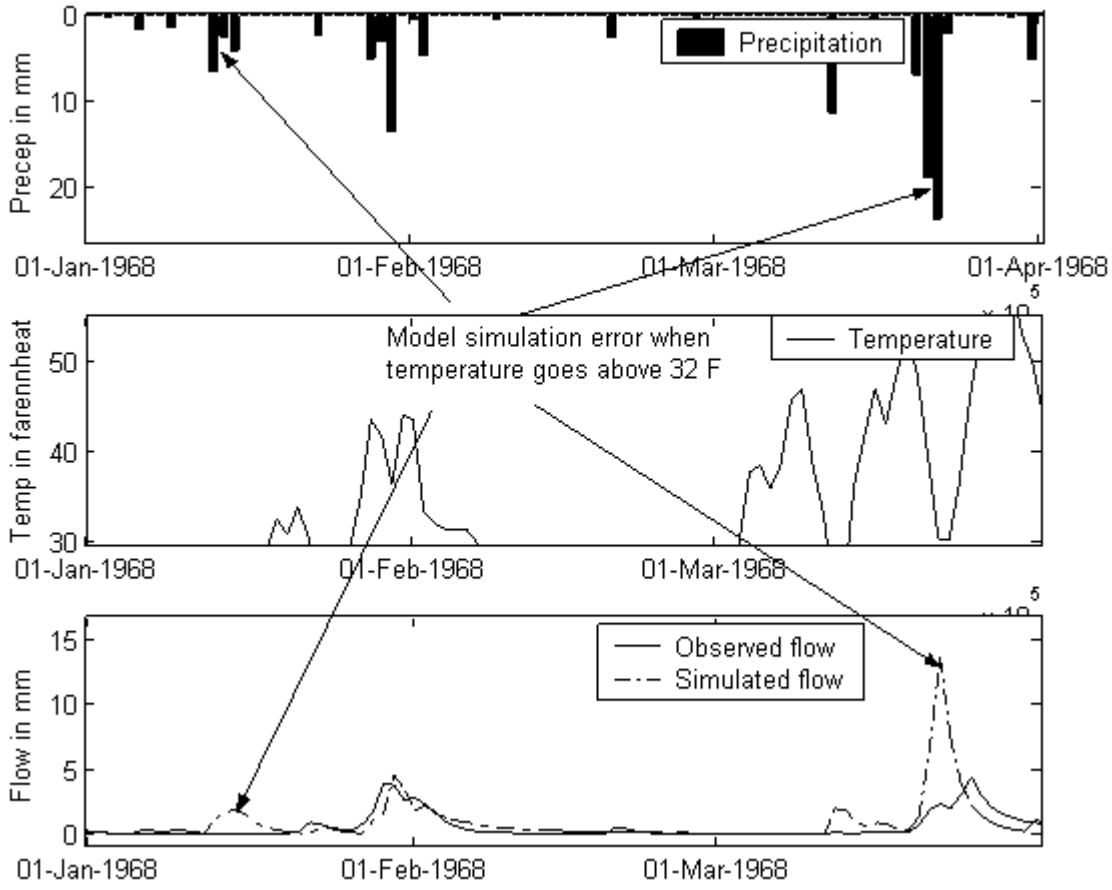

Figure 3.5: Flow and precipitation and temperature before snowmelt model

In Figure 3.6, which shows the simulation for a period of one month from January 1974 to February 1974, we can observe the simulated flow is deviating from the observed flow; this is similarly interpreted as snowmelt. The observed flow between January 13 to January 18 is likely due to snowmelt, since there is a significant rise in temperature above 32^{o} F without any precipitation. The model does not simulate this flow increase because there is no precipitation at that time. So in order to correct this a snowmelt model is needed.

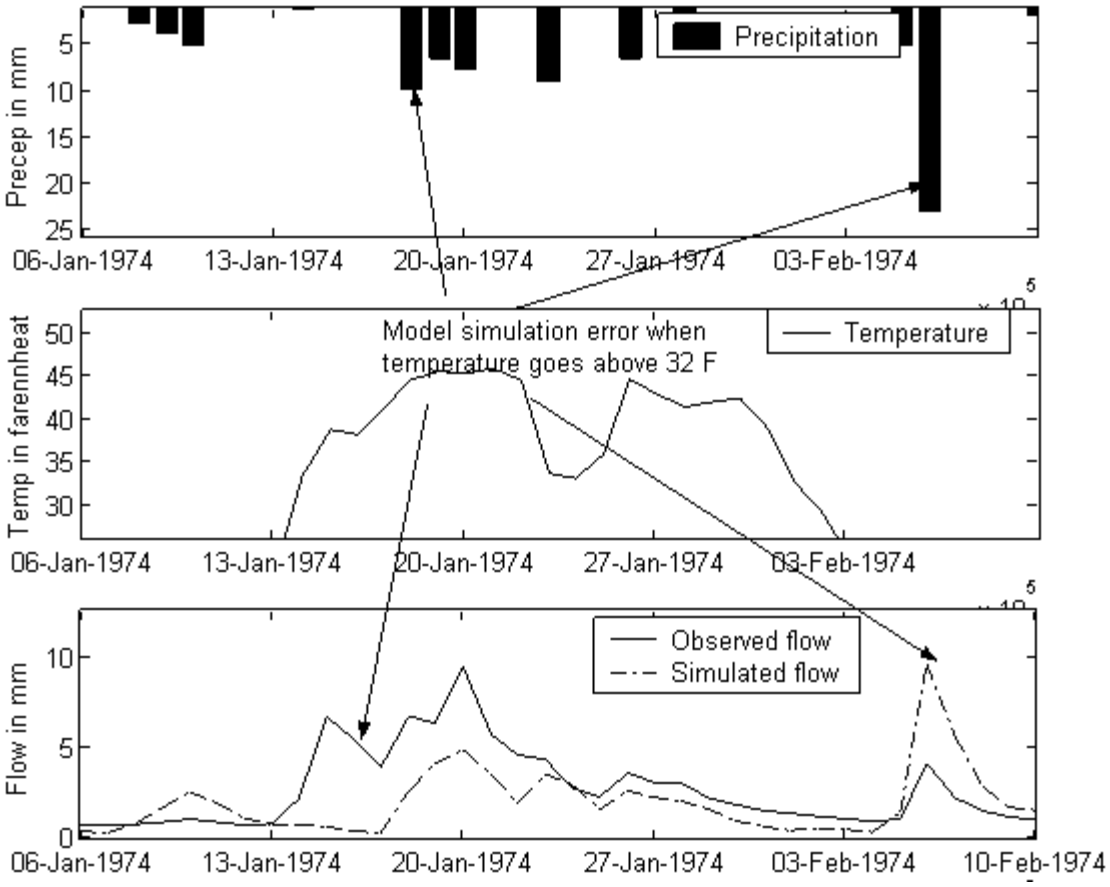

Figure 3.6: Flow and precipitation and temperature before snowmelt model

A simple but widely used, temperature index [21] snowmelt model is implemented to evaluate the effect. Here in the snowmelt model when the temperature is below 32^{o} F all the precipitation on that day is stored as snow and there will be no direct

runoff. The simulated flow that occurs on days with freezing temperatures is only due to the water that drains from the free water. When the temperature is above 32^{o} F some amount of snow is converted to water and it adds to the precipitation on that particular day. Other factors like temperature above the snow, wind, energy balance, slope and aspects of topography, ripening of the snow pack are not taken into consideration in this simple snowmelt model.

The rainfall runoff process is again simulated including the snowmelt model. Figure 3.7 shows the precipitation, temperature, and observed and simulated flow from Jan 1968 to April 1968. The simulated flow more closely matches the observed flow. As the temperature increases the timing and magnitude of simulated flow corresponds much more closely to the actual flow.

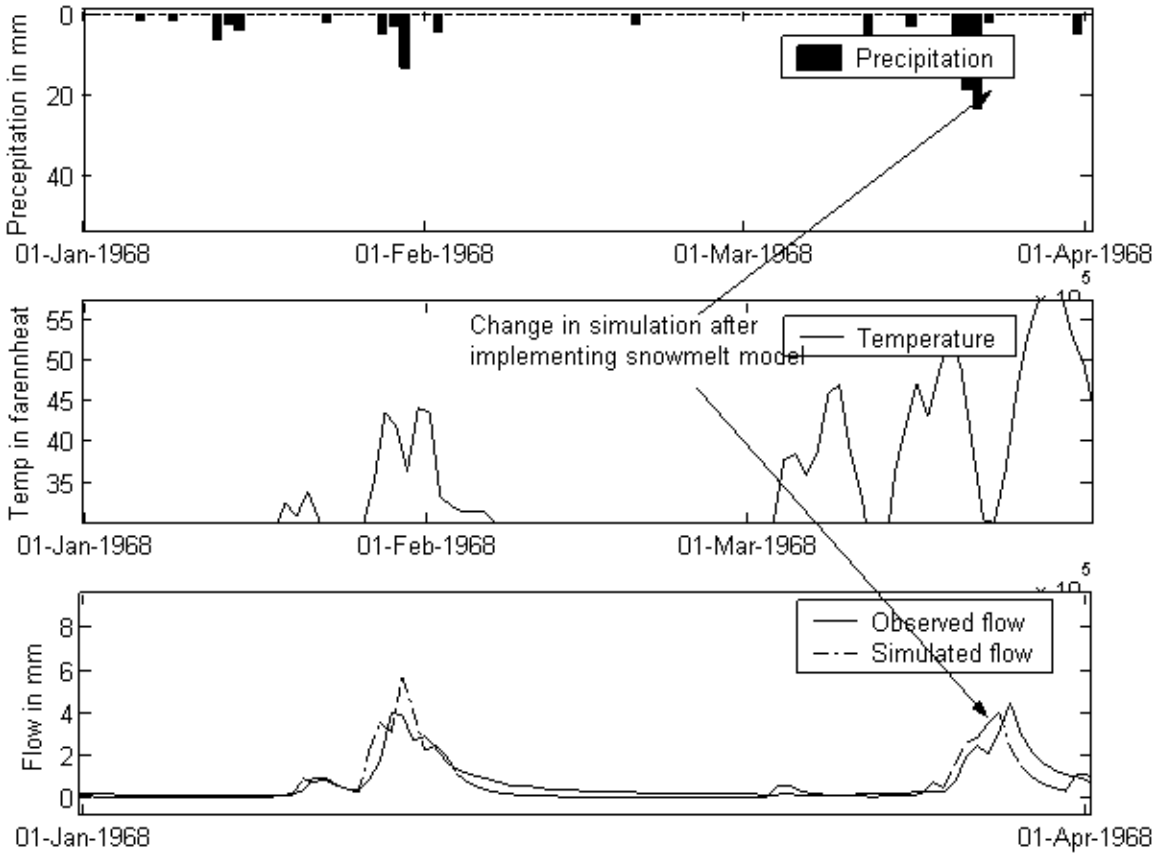

Figure 3.7: Flow, precipitation and temperature after snowmelt model implementation.

In Figure 3.8, between January 13 to January 18, where there is observed snowmelt, simulated flow closely matched the observed flow. But in some cases, as on February 6th where there is runoff below 32° F, the simulated flow deviated from the output, this is because of the other factors [12] that effect the snow melt like wind speed just above the snowmelt, elevation above the sea level, radiation balance, ground temperature, mass of snowpack.

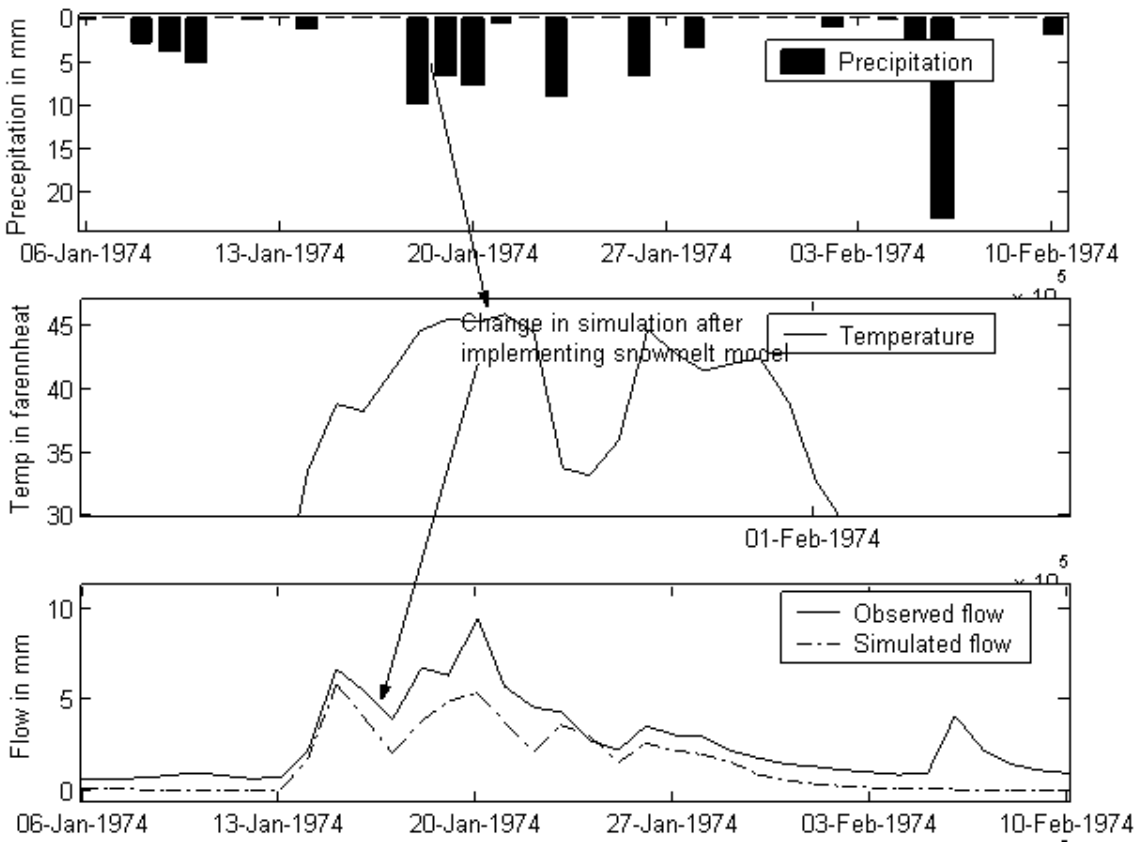

Figure 3.8: Flow, precipitation and temperature after snowmelt model implementation.

After calibration and implementation of channel routing and snow melt model, the model simulations are a very close match to the observed flow. The tables below show the details of calibration and are compared with the simulation of the National Weather Service. Table 3.1 shows the data for the calibrated region 1972 to 1980 and Table 3.2

shows data for the verified region from 1967 to 1975. Here for comparison, the flow data is divided into low flow (for period with less than 0.51 mm of discharge), upper low flow (for discharge between 0.51 mm to 2 mm), medium flow (for period from 2 mm to 8 mm), upper medium flow (for flow between 8 mm to 13 mm), high flows (for flow between 13 mm to 17 mm) and very high flows (for flow exceeding 17 mm). The National Weather Service (without the state updating using just SAC-SMA) simulation and the state space formulation of the Sacramento model coded in Matlab produce almost similar runoff.

Flow in mm	No of days (Observed)	Average Simulated Flow per day in mm	NWS Average Simulated Flow per day in mm	Average Observed Flow per days in mm
<0.51	1724	0.3035	0.3144	0.2203
0.51-2	1132	1.0234	1.0772	1.0046
2-8	378	3.6302	3.5295	3.5789
8-13	38	9.2132	8.1352	9.7653
13-17	8	9.7815	8.6419	14.6819
>17	8	19.1833	16.4223	24.4143

Table 3.1: Flow comparison for calibration period 1972-1980.

Flow in mm	No of days (Observed)	Average Simulated Flow per day in mm	NWS Average Simulated Flow per day in mm	Average Observed Flow per days in mm
<0.51	1841	0.3273	0.3497	0.2230
0.51-2	1044	1.1979	1.1726	1.0054
2-8	360	3.9007	3.7112	3.4817
8-13	30	9.8554	8.8842	10.4060
13-17	7	11.7933	10.6211	15.4246
>17	5	21.3522	20.5653	26.8433

Table 3.2: Flow comparison for simulated period 1967-1975.

In order to improve the simulation optimal filtering techniques are implemented. These filtering techniques are discussed in the next chapter.

CHAPTER IV

OPTIMAL FILTERING TECHNIQUES

Rainfall runoff models are non-linear and time-variant. The errors in a rainfall runoff model are mainly due to limitations of the model itself, parameter uncertainty, accumulation of errors and errors in the input data used for parameter estimation. Hydrological models are very sensitive to the state of the soil: it is a key variable of rainfall transformation into infiltration or runoff. Therefore, a better representation of this variable over the basin should increase the accuracy of the rainfall–runoff process simulation.

The error in the prediction of runoff arises from the uncertainty caused by the physical process, the model and the input data, and can be reduced if optimal filter techniques are incorporated. If the model predictions diverge from the observations at a given time, it will affect the future estimations and chances that the future estimate will approach the correct value is limited. So we need to improve the trajectory of the model

based on the assimilation of observations during the period preceding the time when an immediate or long-term prediction is desired. These observations are assimilated individually in different models: streamflow data are used in runoff and flood forecasting procedures [14, 26] and surface soil moisture data are used in land surface hydrologic models or to constrain soil–vegetation–atmosphere transfer models [27, 28].

The method used is a sequential method: the internal (conceptual) states of the model (soil and routing reservoirs) are corrected using optimal filtering. This methodology consists of locally correcting the value of the internal states of the model when an observation is available. Figure 4.1 shows the principle of estimation with state updating where the state value is updated with a posteriori prediction of the observation. At time *k*, an observation is available. The difference between the observed (black point) and a priori simulated (white point) values is partially corrected and an a posteriori value of the state, closer to the actually observed value, is obtained (gray point). Then the model starts from these new initial conditions and evolves freely until new observations are available. Calculation of the correction factor is an important step of the method: if this factor is too small, the assimilation procedure will have no effect, if it is too large, the model will forget all the past evolution.

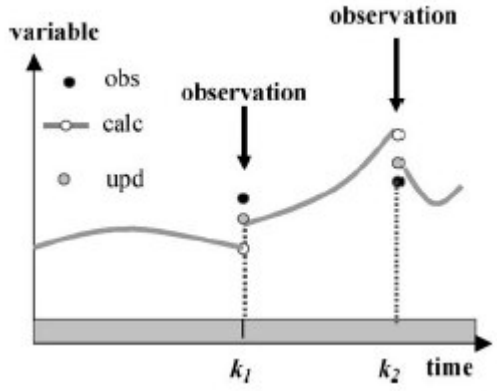

Figure 4.1: Schematic of estimation [37].

In this chapter we will be discussing optimal filtering techniques used in the estimation of the states of the system. The filtering techniques discussed in this chapter are:

1. Kalman filter
2. H-infinity filter.

While the Kalman filter [29] is used previously in the estimation of the streamflow, we will be implementing the H-Infinity filter [31] for estimation of the states and compare the results with that of the Kalman filter. Section 4.1 discusses the Kalman filter, Section 4.2 discusses the H-Infinity filter and Section 4.3 discusses the stability of filters.

4.1 Kalman Filter

4.1.1 Recursive Least Squares Filter

In order to understand the Kalman filter we need to have idea about the recursive least square filter. A recursive filter is one in which we need not store past measurements for evaluating the present estimates. We need measurements at the present time to get the

estimates at the present time. The concept of the recursive filter is best demonstrated below.

Consider the problem of estimating a scalar constant, *x,* based on *k* noise corrupted measurements, which are modeled as follows:

$$z_i = x + e_i \tag{4.1}$$

Where $i = 1,2,3,....k$ and e_i is considered to be white noise. An unbiased, minimum variance estimate can be obtained by averaging all the measurements which is given as:

$$\hat{x}_k = \frac{1}{k}\sum_{i=1}^{k} z_i \tag{4.2}$$

When an additional measurement is available, the new estimate is updated as:

$$\hat{x}_{k+1} = \frac{1}{k+1}\sum_{i=1}^{k+1} z_i$$

In order to use this expression all the measurements before obtaining new measurement have to be stored. But manipulating this equation by including previous estimate, the need to store all the measurements can be avoided. This is shown as follows:

$$\hat{x}_{k+1} = \frac{1}{k+1}\left(\sum_{i=1}^{k} z_i\right) + \frac{1}{k+1} z_{k+1} = \frac{k}{k+1}\hat{x}_k + \frac{1}{k+1} z_{k+1}$$

This can be written as

$$\hat{x}_{k+1} = \hat{x}_k + \frac{1}{k+1}\left(z_{k+1} - \hat{x}_k\right) \tag{4.3}$$

The above equation can be termed as recursive linear estimator and $\left(z_{k+1} - \hat{x}_k\right)$ known as the measurement residual in the above equation [32]. It can be easily understood from the last part of the above equation that the new estimate is given by the previous estimate

plus a weighted difference between the new measurement and its expected value. This weighting factor for the measurement residual is called the estimator gain. The above equation holds good for the scalar case. The process can be directly applied to vector quantities. Let us now consider the case with vector quantity. The vector notation for the measurements available is given as follows:

$$z_k = H_k x + e_k \tag{4.4}$$

Here, x = constant unknown vector that needs to be estimated, z_k is the k^{th} measurement vector and H_k is the observation matrix at the k^{th} time step and e_k is the noise or the error vector. From Equation 4.3, the estimate at the present time is given as [32]:

$$\hat{x}_k = \hat{x}_{k-1} + K_k(z_k - H_k\hat{x}_{k-1}) \tag{4.5}$$

Where K_k is the estimator gain matrix that has to be determined and $(z_k - H_k\hat{x}_{k-1})$ is called the correction term, which is similar to the measurement residual in the scalar case. The estimation error can be defined as the difference between the unknown vector and the estimate at the present time given by

$$\varepsilon_{x,k} = x - \hat{x}_k$$

Taking the expected value of the estimation error we get,

$$\begin{aligned} E(\varepsilon_{x,k}) &= E(x - \hat{x}_k) \\ &= E(x - \hat{x}_{k-1} - K_k(z_k - H_k\hat{x}_{k-1})) \\ &= E(x - \hat{x}_{k-1}) - K_k E(H_k x + e_k - H_k\hat{x}_{k-1}) \\ &= (I - K_k H_k)E(\varepsilon_{x,k-1}) - K_k E(e_k) \end{aligned} \tag{4.6}$$

This estimation can be termed as unbiased because the expected value of the estimate can be proved to be equal to the expected value of the actual unknown quantity. So it can prove with couple of assumptions. They are:

$$E(\varepsilon_{x,k}) = E(x - \hat{x}_{k-1}) = 0 \text{ if } E(e_k) = 0$$

Here we assuming the measurement noise (e_k) to be zero mean and the average estimation error to be zero. The estimate obtained with these conditions is an unbiased estimate since the expected value of the estimate is equal to the expected value of the true value.

The cost function of the estimator can be defined as:

$$J = \tfrac{1}{2} E(\varepsilon_{x,k}{}^T \varepsilon_{x,k})$$

$$= \tfrac{1}{2} Tr\left\{E(\varepsilon_{x,k}\varepsilon_{x,k}{}^T)\right\} \quad \text{Where } Tr \text{ represent s the trace of matrix}$$

$$= \tfrac{1}{2} Tr(P_k)$$

where $P_k = E(\varepsilon_{x,k}\varepsilon_{x,k}{}^T)$

$$= E\left[\left\{(I - K_k H_k)\varepsilon_{x,k-1} - K_k e_k\right\}\left\{(I - K_k H_k)\varepsilon_{x,k-1} - K_k e_k\right\}^T\right]$$

$$= (I - K_k H_k) P_{k-1} (I - K_k H_k)^T + K_k R K_k^T \qquad (4.7)$$

Here R is covariance of measurement noise vector, which is assumed to be zero mean and the above equation, represents estimator error covariance. Minimizing the cost function J with respect to the estimator gain and equating it to minimum (zero) would give the value of the optimal estimator gain, i.e., we need to evaluate the partial of the cost function with respect to gain and make it equal to zero.

$$\frac{\partial J_k}{\partial K_k} = \frac{1}{2}\left[\frac{\partial}{\partial K_k} Tr(I - K_k H_k) P_{k-1} (I - K_k H_k)^T + \frac{\partial}{\partial K_k} Tr(K_k R_k K_k^T)\right]$$

$$= \tfrac{1}{2}\left[2(I - K_k H_k) P_{k-1} (-H_k)^T + 2 K_k R_k\right] \qquad (4.8)$$

From the above equation we get:

$$K_k = P_{k-1} H_k^T (H_k P_{k-1} H_k^T + R_k)^{-1} \qquad (4.9)$$

The above equation represents estimator gain. These results could be used to non-linear systems. But the non-linear systems have to be linearized and the change in the states has to be estimated. Considering a linear discrete time varying system

$$x_k = A_{k-1}x_{k-1} + B_{k-1}u_{k-1} + \Lambda_{k-1}w_{k-1} \tag{4.10}$$

where u_{k-1} is known input to the system, w_k is a gaussian random variable with zero mean and covariance Q_k .

The initial condition of state x_0 is a Gaussian random variable with its mean and covariance matrix as:

$$E(x_0) = m_0$$

$$E\left[(x_0 - m_0)(x_0 - m_0)^T\right] = P_0 \tag{4.11}$$

The state is propagated through the time by

$$E(x_k) = m_k = E(A_{k-1}x_{k-1} + B_{k-1}u_{k-1} + \Lambda_{k-1}w_{k-1})$$

$$= A_{k-1}m_{k-1} + B_{k-1}u_{k-1} \tag{4.12}$$

Here $E(w_{k-1}) = 0$ and $E(u_{k-1}) = u_{k-1}$ from the previously made assumptions. The propagation of covariance is described as:

$$P_k = E\left[(x_k - m_k)(x_k - m_k)^T\right]$$

The product of the state perturbations as present time is given as

$$(x_k - m_k)(x_k - m_k)^T = \left[A_{k-1}(x_{k-1} - m_{k-1}) + B_{k-1}(0) + \Lambda_{k-1}w_{k-1}\right]$$

$$\left[A_{k-1}(x_{k-1} - m_{k-1}) + B_{k-1}(0) + \Lambda_{k-1}w_{k-1}\right]^T$$

$$P_k = E\left\{\left[A_{k-1}(x_{k-1} - m_{k-1}) + \Lambda_{k-1}w_{k-1}\right]\left[A_{k-1}(x_{k-1} - m_{k-1}) + \Lambda_{k-1}w_{k-1}\right]^T\right\}$$

$$= E\{A_{k-1}(x_{k-1} - m_{k-1})(x_{k-1} - m_{k-1})^T A_{k-1}^T$$

$$+A_{k-1}w_{k-1}w_{k-1}^{T}A_{k-1}^{T}+A_{k-1}(x_{k-1}-m_{k-1})w_{k-1}^{T}\Lambda_{k-1}^{T}$$
$$+A_{k-1}w_{k-1}(x_{k-1}-m_{k-1})^{T}A_{k-1}^{T}\}$$

As $E(w_{k-1}w_{k-1}^{T})=Q_{k-1}$ and $E(w_{k-1}x_{k-1}^{T})=0$ the final value is

$$P_k = A_{k-1}P_{k-1}A_{k-1}^{T}+\Lambda_{k-1}Q_{k-1}\Lambda_{k-1}^{T} \tag{4.13}$$

This in one of the important equation as it describes the propagation of estimation error covariance in time.

4.1.2 Discrete Time Kalman Filter

In the previous section, estimation algorithm for measurement systems was described where the state estimate is specified by its conditional probability density function. The purpose of a filter is to compute the state estimate, while an optimal filter minimizes the spread of the estimation error probability density. A recursive optimal filter propagates the conditional probability density function from one sampling instant to the next, taking into account system dynamics and inputs, and it incorporates measurements and measurement error statistics in the estimate. As discussed in the previous section, the state estimate is specified by expected value of the true state's conditional probability density function and the spread of uncertainty in estimate is specified as the covariance matrix. This recursive generation of the mean and covariance in finite time can be explained in the following five steps:

1. State Estimate Extrapolation (Time Propagation)

2. Covariance Estimate Extrapolation (Time Propagation)

3. Filter Gain Computation

4. State Estimate Measurement Update

5. Covariance Estimate Measurement Update

The first two steps that describe the propagation of the estimate of the state and its uncertainty (estimation error covariance) are already discussed in the previous section. The last three steps can be performed by the recursive least squares estimation technique. To derive the mathematical form of the five steps mentioned above in order to derive the Kalman filter, a linear time varying discrete time system is considered, which is represented by

$$x_k = A_{k-1}x_{k-1} + B_{k-1}u_{k-1} + \Lambda_{k-1}w_{k-1} \tag{4.14}$$

$$z_k = C_k x_k + e_k \tag{4.15}$$

Here the first equation represents state equation of the system where x is a state vector, u is the control vector, and w is the process noise, which is zero-mean Gaussian random variable. Here

$$E(w_k) = 0$$

$$E(w_k w_k^{\ T}) = Q_k \tag{4.16}$$

The above equation describes the measurement model of the system z. The measurement vector is a combination of state x with some measurement noise e. This noise e is also a Gaussian random variable with R_k as its covariance.

$$E(e_k) = 0$$

$$E(e_k e_k^T) = R_k \tag{4.17}$$

Implementing the results from the previous section, we derive the Kalman filter equations. Here one must distinguish between the estimates made before the measurements are processed at time instant k and after the measurements are processed at

that instant. The superscript $(-)$ represents the state estimate and covariance before the measurement is processed and (+) represents their values after measurement is processed. From previous section the state estimate is given by

$$\hat{x}_k^- = A_{k-1}\hat{x}_{k-1}^+ + B_{k-1}u_{k-1} \tag{4.18}$$

The covariance estimate is given by

$$P_k^- = A_{k-1}P_{K-1}^+A_{k-1}^T + \Lambda_{k-1}Q_{k-1}\Lambda_{k-1}^T \tag{4.19}$$

The filter gain is given by

$$K_k = P_k^-C_k^T\left[C_kP_k^-C_k^T + R_k\right]^{-1} \tag{4.20}$$

From previous section the updated equations after the measurements are processed is given as

$$\hat{x}_k^+ = \hat{x}_k^- + K_k(z_k - C_k\hat{x}_k^-) \tag{4.21}$$

$$P_k^+ = (I - K_kC_k)P_k^-(I - K_kC_k)^T + K_kR_kK_k^T \tag{4.22}$$

These are the basic Kalman filter equations.

4.1.3 Continuous Time Kalman Filter

Considering a non-linear system, the Kalman filter is used by modifying the condition of optimality from that of the linear systems. The non-linear system is represented as:

$$\dot{x} = f(x,u,w,t)$$
$$z = h(x,t) + e(t)$$

Here x is the state vector, u is the input, w and e are the process and measurement noises with covariances Q and R respectively.

The system must be linearized about a nominal operating condition in order to implement Kalman filter. By expanding the non-linear system by Taylor series

$$\hat{x} \approx f(x_0, u_0, w_0, t) + \frac{\partial f}{\partial x}\Big|_0 (x - x_0) + \frac{\partial f}{\partial u}\Big|_0 (u - u_0) + \frac{\partial f}{\partial w}\Big|_0 (w - w_0)$$

$$z \approx h(x_0, t) + \frac{\partial f}{\partial x}\Big|_0 (x - x_0) + e(t)$$

where $\frac{\partial ..}{\partial ..}\Big|_0$ represents the corresponding partial derivative evaluated at x_0, u_0, w_0 which are nominal values. The partial fractions in the above equations can be expressed as $F = \frac{\partial f}{\partial x}, G = \frac{\partial f}{\partial u}, L = \frac{\partial f}{\partial w}, H = \frac{\partial h}{\partial x}$. So the linearized equations are represented as

$$\dot{x} = f(x_0, u_0, w_0, t) + F(x - x_0) + G(u - u_0) + L(w - w_0)$$
$$z = h(x_0, t) + H(x - x_0) + e(t)$$

Considering

$$\dot{x} = f(x_0, u_0, w_0, t), z_0 = h(x_0, t)$$

$$w_0 = 0$$

$$x - x_0 = \Delta x$$

$$u - u_o = \Delta u$$

$$w - w_0 = \Delta w$$

$$z - z_0 = \Delta z$$

$$\dot{x} - \dot{x}_0 = \Delta \dot{x}$$

the non-linear system can be represented as

$$\Delta \dot{x} = F\Delta x + G\Delta u + Lw \qquad (4.23)$$

$$\Delta z = H\Delta x + e \qquad (4.24)$$

The standard Kalman filter can be applied to the linear system and states can be estimated. The modified equations are

$$\Delta\dot{\hat{x}} = F\Delta x + K(\Delta z - H\Delta\hat{x}) \tag{4.25}$$

$$K = PH^T R^{-1} \tag{4.26}$$

$$\dot{P} = FP + PF^T + LQL^T - PH^T R^{-1} HP \tag{4.27}$$

The true state estimate can be calculated by summing the estimated change in states to the nominal states as shown

$$\hat{x} = x_0 + \Delta\hat{x} \tag{4.28}$$

The linearized Kalman filter doesn't give exact optimal estimates, but they would be near to the optimum values, i.e., an approximate optimal estimate, as they are based on the nominal trajectory.

4.2 H-infinity Filter

In the above section the Kalman filter is derived assuming the measurement error is zero-mean. But in many cases the error is not a zero mean. At that point we can use an H-infinity filter. The H-infinity estimator is called the minmax filter as it tries to minimize the worst-case gain from the noise to estimation error. The H-infinity filter does not make any assumptions about the noise. Consider a nonlinear system of the form

$$\dot{x} = f(x) + Bw + \varepsilon$$
$$y = h(x) + e$$

Here x is the state vector, y is the measurement, w and e are the uncorrelated unity variance white noise sequence, ε is an arbitrary noise sequence, y is the observer vector. f and h are the non-linear functions of state. Noise vector and the estimation error are defined as follows:

$$\delta = \begin{bmatrix} w^T v^T \end{bmatrix}^T \tag{4.29}$$

$$\varepsilon_x = x - \hat{x} \tag{4.30}$$

H- infinity filter is used to find an estimate $\hat{x}$ such that the infinity norm of the transfer function from the augmented noise vector δ to the estimation error ε_x is bounded by a user defined quantity.

$$|| T_{\varepsilon_x e} ||_\infty < \gamma \tag{4.31}$$

where $T_{\varepsilon\delta}$ is the transfer function from δ to ε_x. The above equation means that the maximum steady state gain from δ to ε_x should be less than the user-defined value γ. The cost function of the estimator can be defined as

$$J = \sup_{w \neq 0} \frac{\left\| x - \hat{x} \right\|_2}{\left\| w \right\|_2} \tag{4.32}$$

The desired estimate $\hat{x}$ can be obtained by the using recursive H-infinity estimator. In order to implement the H-infinity estimator the system is written as shown below

$$\dot{x} = Ax + Bu + B_w w \tag{4.33}$$

$$m = C\ x + D\ u + D_w w \tag{4.34}$$

$$y = C_y x \tag{4.35}$$

where m is the measured signal. The H-infinity estimator equations are given as follows.

$$\Delta\dot{\hat{x}} = A\Delta x + B\Delta u + K(\Delta m - C_k \Delta\hat{x} - D_k \Delta u) \tag{4.36}$$

$$K = QC^T \tag{4.37}$$

$$\dot{Q} = QA^T + AQ + B_w B_w^T - Q(C^T C\ - \gamma^{-2} C_y^T C_y)Q \tag{4.38}$$

$$\Delta x = \Delta x + \Delta \dot{x}\, dt \tag{4.39}$$

$$\hat{x} = x_0 + \Delta\hat{x} \tag{4.40}$$

where K is the H-infinity estimator gain matrix and Q is the solution to the Riccati equation.

4.2 Relation between Kalman Filter and H-infinity Filter

Kalman filter can be implemented using the H-infinity filter equations [31]. H-infinity filter is used to find an estimate $\hat{x}$ such that the infinity norm of the transfer function from the augmented noise vector e to the estimation error ε_x is bounded by a user defined quantity, as shown in equation 4.31. When this user defined quantity is infinity the H-infinity filter behaves like the Kalman filter. This is well explained in [31, 33]

$$|| T_{\varepsilon_x e} ||_\infty < \infty \tag{4.41}$$

In such case Equation 4.38 can be written as

$$\dot{Q} = QA^T + AQ + B_w B_w{}^T - Q(C^T C)Q \tag{4.42}$$

4.3 Stability of Filters

In this thesis we are not trying to prove the stability of the system but we are actually trying to get a good estimate of the states using state estimation. Stability is extremely difficult to prove for nonlinear filters, requiring a number of assumptions on the magnitudes of the inputs and nonlinearities. Stability of a system can be proven theoretically, but it cannot be demonstrated via simulation. A stable system is one that has bounded output for a bounded input. So we expect a stable filter [34, 35] to have a

bounded state estimate. An unstable system can also have a bounded state estimate, depending on the inputs to the filter. In general, a heuristic approach must be taken to stability for nonlinear filters. That is, nonlinear filters are generally tuned to give good performance, but theoretical stability is not proven. For some theoretical work on nonlinear Kalman filter stability, see [38].

The convergence of the filter is another issue that is important but that we do not address in this thesis. This is different than stability. Stability means that the estimation error remains bounded, but convergence means that the mean of the estimation error approaches zero. For some theoretical work on nonlinear Kalman filter convergence, see [50].

CHAPTER V

SIMULATION RESULTS

The main aim of this thesis is to implement optimal filtering techniques for state updating in a continuous hydrologic simulation model, and to evaluate their performance and utility for improved streamflow prediction. Previously the Kalman filter has been used in state estimation in streamflow forecasting [13]. In this work both the Kalman filter and the H-infinity filter are implemented for state estimation.

This chapter describes with the simulated results obtained after implementation of both the filters. These results are obtained after calibrating the model for a period from 1972 to 1980 and verifying this calibration from 1967 to 1975. The results that are obtained are compared to both observed streamflow and the simulation results of the National Weather Service. Section 5.1 gives information on the results obtained for SS-SAC-SMA model calibration and verification. Section 5.2 describes with the results obtained from the state updating with the Kalman filter and the H-infinity filter and Section 5.3 compares the two filters. The simulation results are evaluated by the water

balance, correlation with the observed flow and using the Nash Sutcliffe Coefficient [39, 40]. The Nash Sutcliffe Coefficient is to measure of the fit between the predicted and measured values. The computation of coefficient of efficiency (*E*) is essentially is the sum of the deviation of the observations from a linear regression line with slope of 1. If the measured value is same as all the prediction then *E* is 1. The value of *E* lies between 0 and 1, which indicates deviation between the measured and the predicted value. If the value of *E* is negative then the predictions are very poor and the average value of the output is better estimate than the model prediction. There are many forms of The Nash Sutcliffe coefficient (*E*) that can be used for performance measure. Two of the methods are given below

The Nash Sutcliffe coefficient (*E*) is relative to the mean observed flow is computed as:

$$E_{mean} = \frac{\sum_{i=1}^{n}(Q_{m,i} - Q_{mean})^2 - \sum_{i=1}^{n}(Q_{m,i} - Q_{p,i})^2}{\sum_{i=1}^{n}(Q_{m,i} - Q_{mean})^2}$$

where, E_{mean} is the coefficient of efficiency calculated taking the mean observed flow as a mean reference.

$Q_{m,i}$ is the measured value on i^{th} day.

$Q_{p,i}$ is the predicted value on i^{th} day.

Q_{mean} is the arithmetic average measured value.

The Nash Sutcliffe coefficient (*E*) is computed taking previous day observed flow is given as:

$$E_{Persistence} = \frac{\sum_{i=1}^{n}(Q_{m,i} - Q_{m,i-1})^2 - \sum_{i=1}^{n}(Q_{m,i} - Q_{p,i})^2}{\sum_{i=1}^{n}(Q_{m,i} - Q_{m,i-1})^2}$$

where, $E_{Persistence}$ is the coefficient of efficiency calculated taking relative to the previous days observed flow data as reference. This is also called persistence forecast reference.

5.1 SS-SAC-SMA Model Simulation Results

The model is calibrated for a period from 1972 to 1980 and then it is used for prediction from 1967 to 1975. The calibration results from 1972 to 1980 are summarized in Table 5.1. This table has five fields with number of days where the streamflow is in a given range, average simulated streamflow per day, average observed streamflow by USGS per day and error in simulation of the flow when it is compared to the observed flow. Here for comparison, the flow data is divided into low flow (for period with less than 0.51 mm of flow data), upper low flow (for flow between 0.51 mm to 2 mm), medium flow (for period from 2 mm to 8 mm), upper medium flow (for flow between 8 mm to 13 mm), high flows (for flow between 13 mm to 17 mm) and very high flows (for flow exceeding 17 mm). As the table summarizes, the calibration period contained 1724 days with less than 0.51 mm of runoff and 1132 days within the period between 0.51 mm to 2 mm of runoff, 378 days with less than 8 mm of runoff, 38 days with flow between 8 mm to13 mm, 8 days with flow between 13 mm and 17 mm and 8 days with flow greater than 17 mm. Here the simulated model is producing more runoff when there is a very low flow and producing less water when there is high flow. The Nash Sutcliffe Coefficient is

0.73 and persistence measure is 0.48. The cumulative water error i.e. the difference in the cumulative observed and simulated flow for the nine-year period is 20 mm.

Flow in mm	No of days	Average Simulated Flow per day in mm	Average Observed Flow per days in mm	Error in %	Simulation Details
<0.51	1724	0.3035	0.2203	-37.7	Cumulative Observed flow = 3553.8 mm
0.51-2	1132	1.0234	1.0046	1.7	Cumulative Simulated flow = 3573.8 mm
2-8	378	3.6302	3.5789	1.3	
8-13	38	9.2132	9.7653	5.4	E_{mean} =0.73 $E_{persistence}$ = 0.48
13-17	8	9.7815	14.6819	32.6	
>17	8	19.1833	24.4143	21.7	Cumulative Water Error =20 mm Correlation=0.81

Table 5.1: State space form of SAC-SMA simulated in Matlab for 1972−1980 without filter

Table 5.2 gives the results that are obtained from the National Weather Service (NWS) simulation. From the table it can be seen that the NWS model, even though it has better Nash Sutcliffe Coefficient, persistence measure and correlation than that of the state space form of Sacramento model deterministic calibration, is producing around 42% more than the actual flow in the low flow period and has high errors in the high flow days.

Flow in mm	No of days	Average Simulated Flow per day in mm	Average Observed Flow per days in mm	Error in %	Simulation Details
<0.51	1724	0.3144	0.2203	-42.7	Cumulative Observed flow = 3553.8 mm Cumulative Simulated flow = 3614.2 mm E_{mean} = 0.75 $E_{persistence}$ = 0.57 Cumulative Water Error =60 mm Correlation=0.85
0.51-2	1132	1.0772	1.0046	7.2	
2-8	378	3.5295	3.5789	1.4	
8-13	38	8.1352	9.7653	16.7	
13-17	8	8.6419	14.6819	41.1	
>17	8	16.4223	24.4143	32.7	

Table 5.2: NWS data Simulated for period 1972 to 1980

Using the model calibrated using 1972 to 1980 data for period of nine years, it is then verified to a different set of years starting from 1967 to 1975. Table 5.3 shows the simulation results. The calibrated model produced 461 mm more streamflow for nine years when compared to the observed flow. This may be because of several reasons like lack of correct input data or changes in the vegetation etc. Here the calibrated state space form of Sacramento model is producing more streamflow for low flow days and less flow on high flow days. The majority of the over simulation is from events less than 2 mm of flow. This is one good example where optimal filtering techniques can be implemented to update the soil moisture states based on the output may reduce the extra flow.

Flow in mm	No of days	Average Simulated Flow per day in mm	Average Observed Flow per days in mm	Error in %	Simulation Details
<0.51	1841	0.3273	0.2230	–46.8	Cumulative Observed flow = 3268 mm Cumulative Simulated flow = 3730 mm $E_{mean} = 0.69$ $E_{persistence} = 0.53$ Cumulative Water Error = 461 mm Correlation = 0.86
0.51-2	1044	1.1979	1.0054	–19.1	
2-8	360	3.9007	3.4817	–12.0	
8-13	30	9.8554	10.4060	6.3	
13-17	7	11.7933	15.4246	23.5	
>17	5	21.3522	26.8433	20.5	

Table 5.3: State space form of SAC-SMA Simulated in Matlab for 1967 to 1975 without filter

Table 5.4 summarizes the results obtained by National Weather Service simulated model. For the verification period, the NWS calibration is producing approximately 380 mm more flow than is observed. Compared to the state space form of Sacramento model, the NWS Sacramento model calibration produces higher low flows than the calibrated state space form of Sacramento model. For the period from 1967 to 1975 it can be seen that both state space calibration of the Sacramento model and NWS calibrated Sacramento model significantly over simulated runoff. Here it is expected that implementing optimal filtering techniques in order to update the states of the system may reduce the errors.

Flow in mm	No of days	Average Simulated Flow per day in mm	Average Observed Flow per days in mm	Error in %	Simulation Details
<0.51	1841	0.3497	0.2230	–56.8	Cumulative Observed flow = 3268 mm Cumulative Simulated flow = 3647.8 mm $E_{mean} = 0.70$ $E_{persistence} = 0.67$ Cumulative Water Error =380 mm Correlation = 0.88
0.51-2	1044	1.1726	1.0054	–16.1	
2-8	360	3.7112	3.4817	–6.6	
8-13	30	8.8842	10.4060	14.6	
13-17	7	10.6211	15.4246	31.1	
>17	5	20.5653	26.8433	23.4	

Table 5.4: NWS data Simulated for period 1967 to 1975

5.2 Kalman and H-infinity Filter Simulation Results

The previous section summarized the deterministic simulation of the calibrated state space form of Sacramento model and the NWS calibrated Sacramento model. This section deals with the results obtained by implementing the optimal filters. This section deals with the Kalman filter and the H-infinity filter results. These filters are coded and implemented in Matlab. The calibration of the state space version of Sacramento model is discussed in Chapter 3. For the calibrated model the filters are implemented. Here these filters are used to estimate the six conceptual soil moisture states in the system. The γ in the H-infinity filter is set to 80 manually by tuning. Trying to reduce the value of γ

further made the filter unstable. B_w is a 6 x 3 matrix which is manually tuned. The value of B_w is shown below:

$$B_w = \begin{pmatrix} -2.96 & 0 & -0.75 \\ -1.65 & 0 & 0 \\ 0 & 0 & 2 \\ 0 & 0 & 0 \\ 0 & 0 & -3.8 \\ 14 & 0 & 0 \end{pmatrix}.$$

For the Kalman filter, the H-infinity filter equations are used and γ is set to infinity. The B_w values are tuned so that the filter gives a good response to the simulation. The values of B_w for the Kalman filter are shown below.

$$B_w = \begin{pmatrix} -5.3 & 0 & -0.2 \\ -.6 & 0 & 0 \\ 0 & 0 & 1 \\ 0 & 0 & 0 \\ 0 & 0 & -1.3 \\ 1 & 0 & 1.5 \end{pmatrix}$$

The B_w values for the filters that were obtained here were found by manual, heuristic tuning. That is, the qualitative match between filter-predicted and measured streamflow was used as the criterion for tuning B_w. These filters are manually tuned and in the B_w matrix some values are made 0 as they have little effect on the performance of the filter or they are making the filter unstable.

Table 5.5 summarizes the results for the Kalman filter for the calibration period from 1972 to 1980. The Kalman filter has good response for almost all the flow periods. This is the time period for which the model is calibrated. The errors are low for almost all the periods, and cumulative water error is very low.

Flow in mm	No of days	Average Simulated Flow per day in mm	Average Observed Flow per days in mm	Error in %	Simulation Details
<0.51	1724	0.2221	0.2203	-0.8	Cumulative Observed flow = 3553.8 mm
0.51-2	1132	0.9491	1.0046	5.5	Cumulative Simulated flow = 3571.4 mm
2-8	378	3.8653	3.5789	-8.0	
8-13	38	9.5199	9.7653	2.5	E_{mean} = 0.78
13-17	8	11.9430	14.6819	18.7	$E_{persistence}$ = 0.63 Cumulative Water Error =17 mm
>17	8	24.4518	24.4143	-0.2	Correlation = 0.90

Table 5.5: Kalman filter estimation summery simulated for period 1972 to 1980

Table 5.6 gives details about the H-infinity filter model simulation for the calibration period from 1972 to 1980. After implementing the filter the model had good response to the inputs and the there is less error when it is compared to the state space form of Sacramento model without state updating. This helps us understand that after implementing the state estimation the model's streamflow simulation is significantly improved.

.

Flow in mm	No of days	Average Simulated Flow per day in mm	Average Observed Flow per days in mm	Error in %	Simulation Details
<0.51	1724	0.2422	0.2203	–9.9	Cumulative Observed flow = 3553.8 mm
0.51-2	1132	1.0375	1.0046	1.7	Cumulative Simulated flow = 3593.9 mm
2-8	378	3.680	3.5789	3.0	
8-13	38	9.0908	9.7653	5.4	$E_{mean} = 0.81$
13-17	8	9.2265	14.6819	37.2	$E_{persistence} = 0.67$ Cumulative Water Error = 40 mm
>17	8	23.6640	24.4143	3.1	Correlation = 0.90

Table 5.6: H-infinity filter estimation summery simulated for calibration period 1972 to 1980

In the above tables we have the results shown for period from 1972 to 1980, where the model is calibrated. The following tables summarize the implementation of the filter for a period from 1967 to 1975 where the model is verified. Table 5.7 summarizes the simulation of the Kalman filter for the period from 1967 to 1975. Here the model response for the low flow periods is significantly improved. The simulated streamflow significantly underestimates streamflow greater than 13mm. The simulated flow on days with less than 13mm of runoff show low error. The Kalman filter is not consistent in maintaining the water balance (but still better than the calibration without state updating), Nash Sutcliffe Coefficient, persistence measure and correlation when it is compared with the simulated data for the period from 1972 to 1980, which may suggest that the Kalman filter may be over-fit to the calibration period.

Flow in mm	No of days	Average Simulated Flow per day in mm	Average Observed Flow per days in mm	Error in %	Simulation Details
<0.51	1841	0.2406	0.2230	–7.9	Cumulative Observed flow = 3268 mm Cumulative Simulated flow = 3208.5mm $E_{mean} = 0.78$ $E_{persistence} = 0.35$ Cumulative Water Error = –60 mm Correlation = 0.79
0.51-2	1044	0.9795	1.0054	2.6	
2-8	360	3.5877	3.4817	–3.0	
8-13	30	10.1306	10.4062	2.6	
13-17	7	10.8614	15.4246	29.6	
>17	5	14.2044	26.8433	47.1	

Table 5.7: Kalman filter estimation summery simulated for period 1967 to 75

Upon simulating streamflow using the H-infinity filter for period from 1967 to 1975, it had comparatively better response than the model without state updating, improving in all the flow periods shown. Table 5.8 summarizes the filter verification results. For the verification period, the H-infinity filter has nearly same water balance and correlation, persistence measure, and Nash Sutcliffe Coefficient as the calibration period from 1972 to 1980.

Flow in mm	No of days	Average Simulated Flow per day in mm	Average Observed Flow per days in mm	Error in %	Simulation Details
<0.51	1841	0.2645	0.2230	−18.6	Cumulative Observed flow = 33268 mm
0.51-2	1044	1.0419	1.0054	−3.6	Cumulative Simulated flow = 3313.2 mm
2-8	360	3.5520	3.4817	−2.0	
8-13	30	9.3522	10.4062	10.1	$E_{mean} = 0.87$
13-17	7	9.0219	15.4246	41.5	$E_{persistence} = 0.65$ Cumulative Water Error =44 mm
>17	5	23.1252	26.8433	13.9	Correlation = 0.88

Table 5.8: H-infinity filter estimation summery simulated for period 1967 to 1975

5.3 Comparison of Models

This section compares the filtering techniques for the two sets of periods. The Kalman filter calibration does not able to react to the sudden high changes in the observed streamflow. The Nash Efficiency, water balance and the correlation are significantly poorer in the verification period than in the calibration period. Figure 5.1 shows the flow generated by the Kalman filter, the H-infinity filter and the observed flow for different periods in the calibrated. Here, it can be observed that the Kalman filter is reacting slowly to the sudden rise in the streamflow after a prolonged dry period.

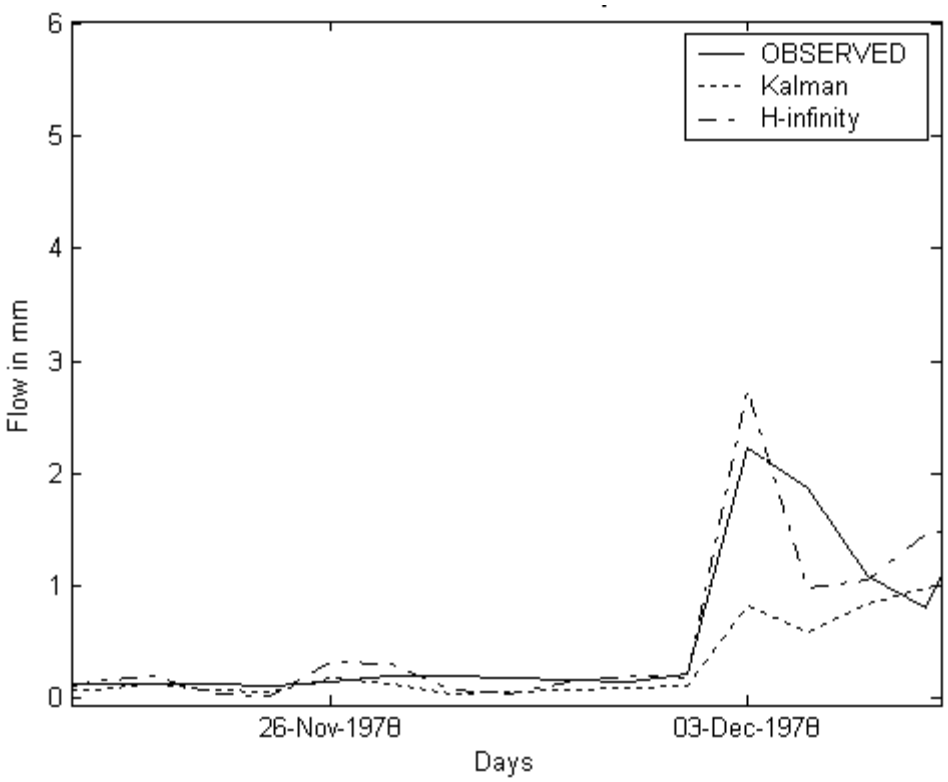

Figure 5.1: Flow comparison for a certain period in calibrated period

Figure 5.2 shows the flow generated by the Kalman filter, the H-infinity filter and the observed flow for the simulated period. This is another example where the Kalman filter did not respond to a sudden increase in the streamflow.

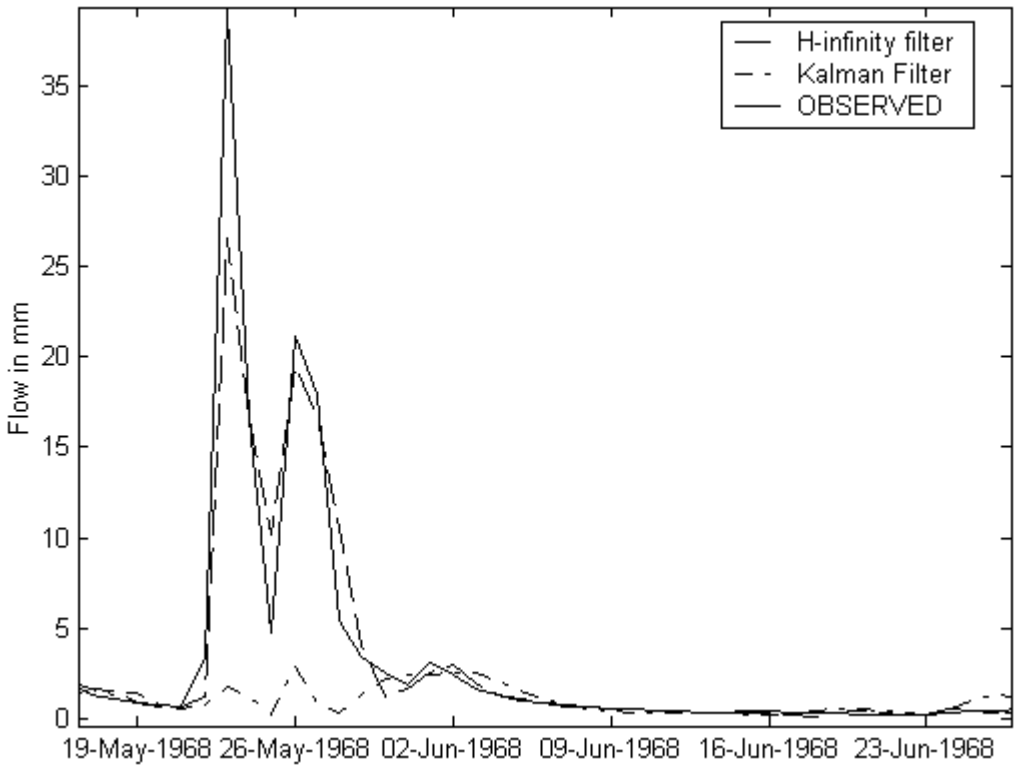

Figure 5.2: Flow comparison for a certain period in simulated period.

The H-infinity filter is producing more flow in the dry season when there is little rainfall and low observed flows. The Kalman filter is closly tracks low flows. Figure 5.3 shows a period in the calibration period where the H-infinity filter is producing more output compared to the flow generated by using the Kalman filter and the observed.

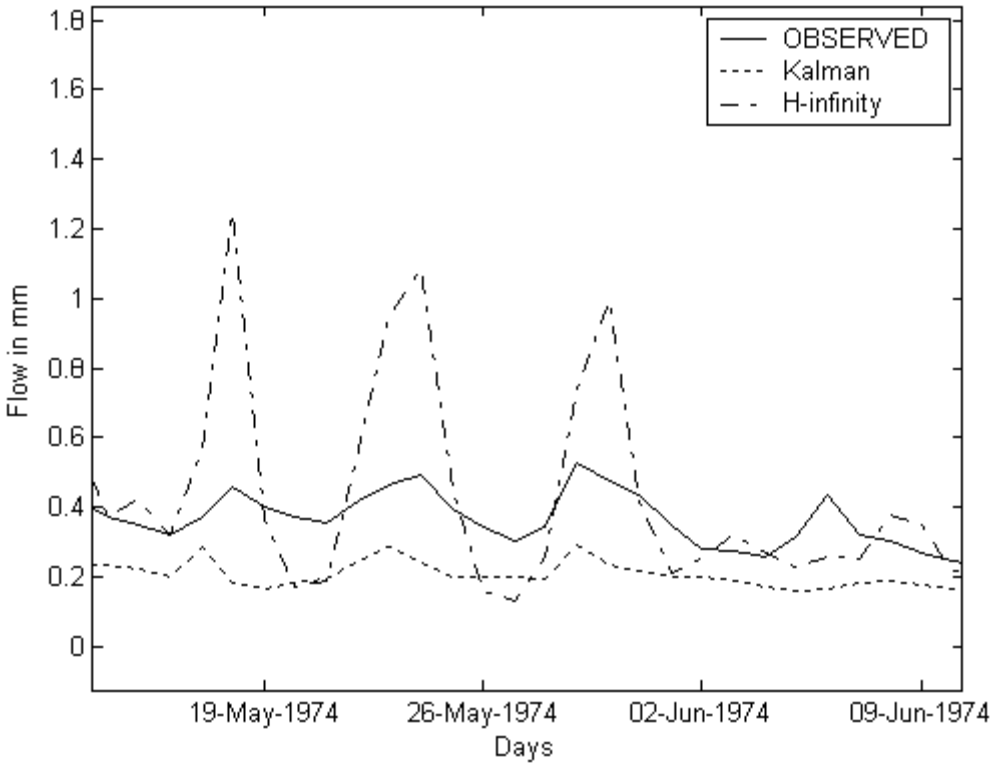

Figure 5.3: Flow comparison for a certain period in calibrated period.

Figure 5.4 similarly shows a period in the verification period where the H-infinity filter is producing more output compared to the flow generated by using the Kalman filter and the observed.

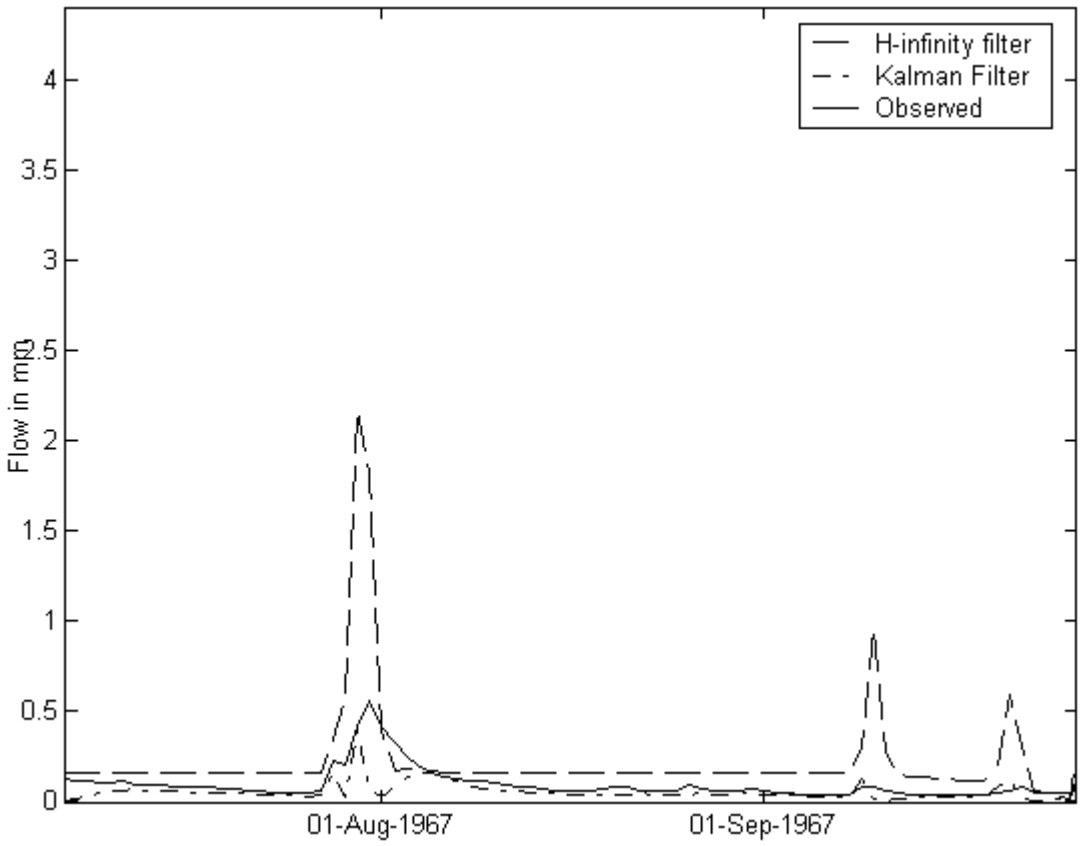

Figure 5.4: Flow comparison for a certain period in calibrated period.

The Kalman filter was under simulating in the low flow periods. The Kalman filter is generating less runoff compared to the observed runoff. Figure 5.5 shows the semilog plot of the flow for a particular period of the record where we can observe that the model is under predicting when it is compared to the actual flow. H-infinity filter has good response when it is compared to the Kalman filter in the low flow periods.

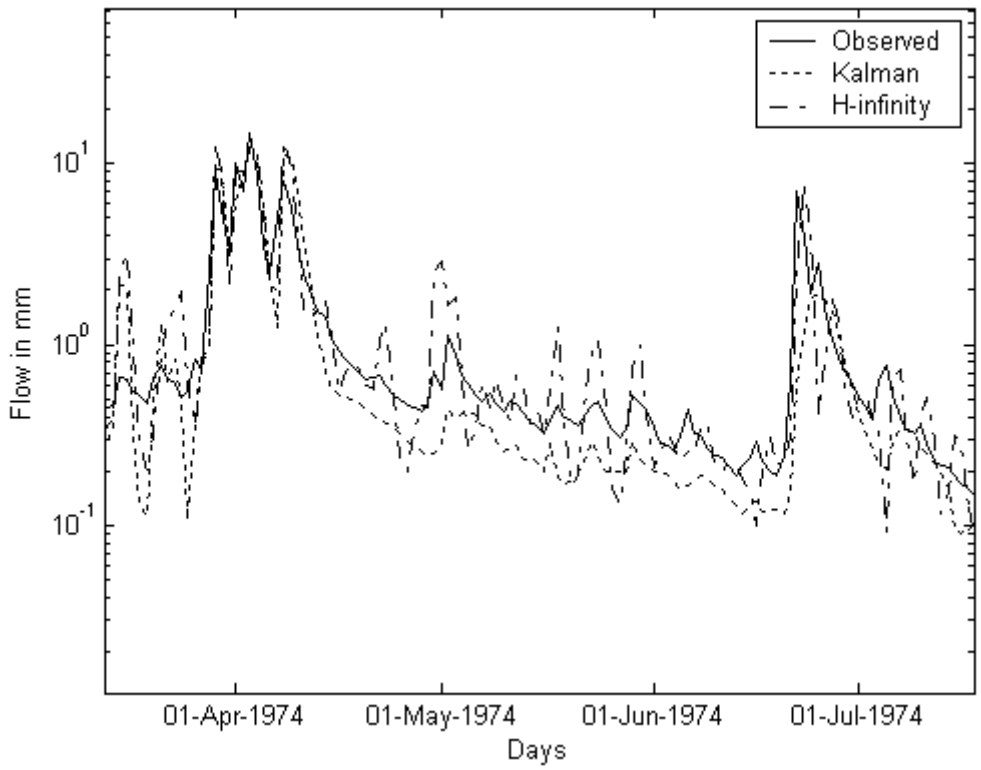

Figure 5.5: Semilog plot of simulated flow.

Figure 5.6 gives details of the average flow simulated with the H-infinity filter on a monthly basis for a period from 1967 to 1975. It can be observed from the data, the months from October to May there are high flows and from month June to September there are low flows. The model responds well for most of the months. But there is some deviation in the months of March and May, which can be due to snowmelt, and the model is also producing less runoff in the months of August and September.

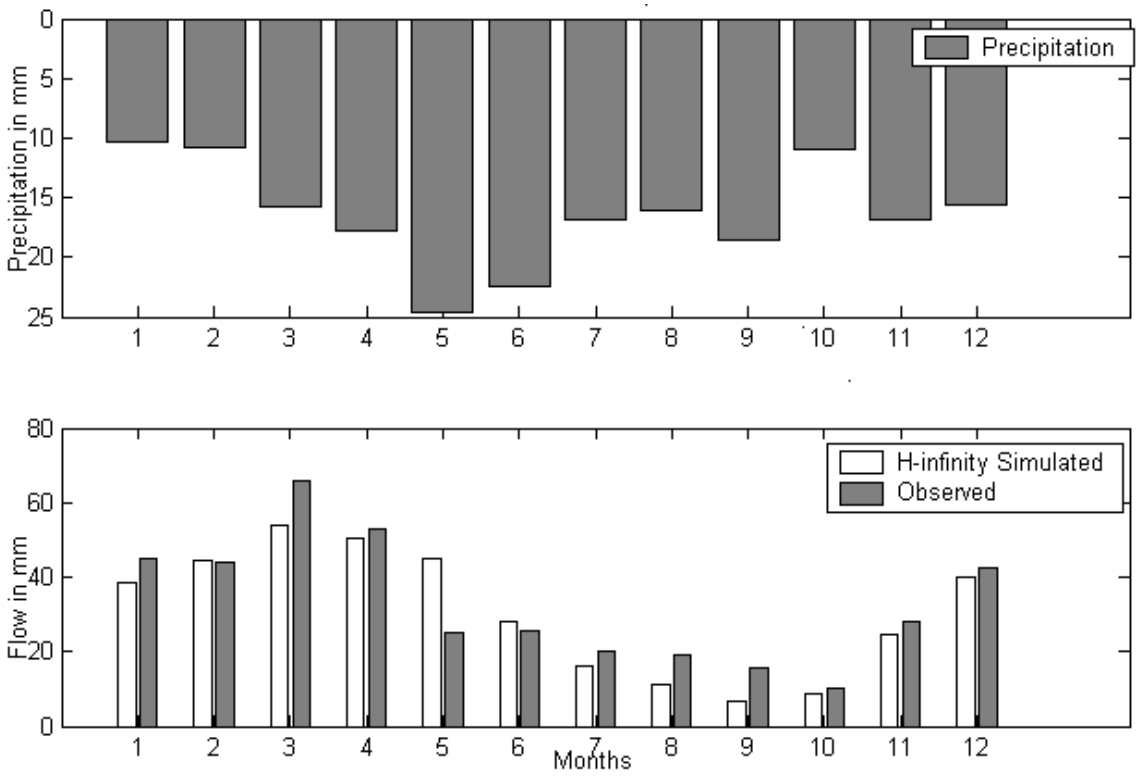

Figure 5.6: Average monthly flow for period from 1967 to 1975 when simulated by H-infinity filter.

Figure 5.7 gives details of the average flow simulated with the Kalman filter on a monthly basis for a period from 1967 to 1975. Here it can be observed from the data the model simulated flow similar to that of the model simulated with the H-infinity filter, but it has better results by producing little less extra flow in the months of May, compared to that of the H-infinity filter.

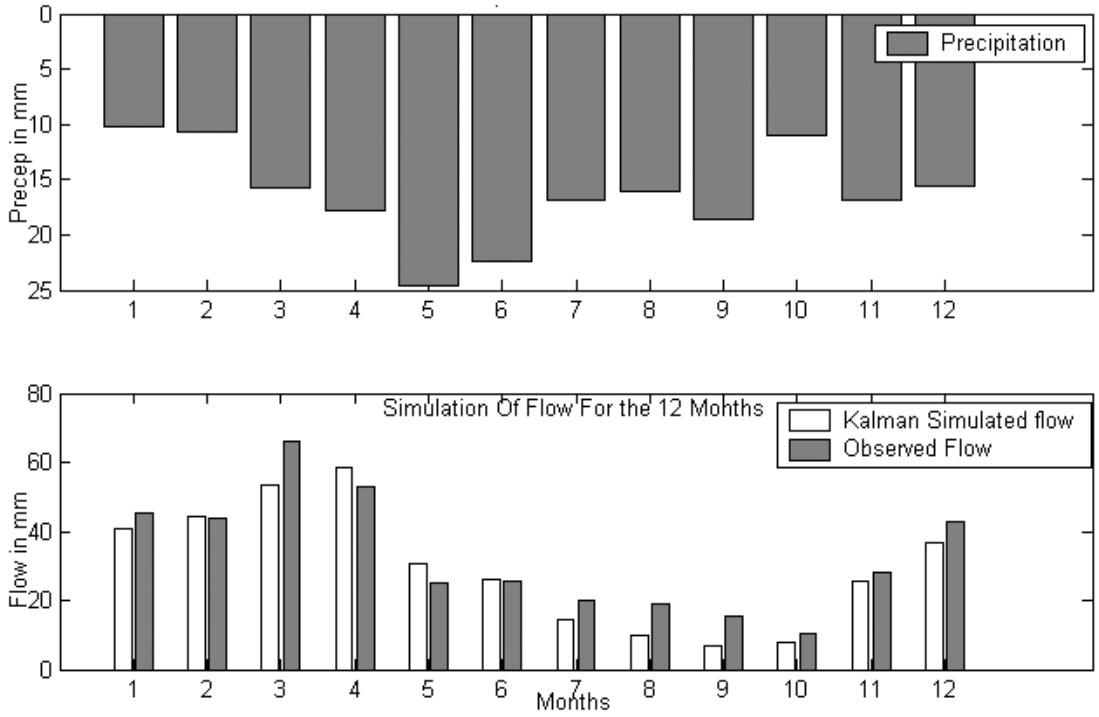

Figure 5.7: Average monthly flow for period from 1967 to 1975 when simulated by Kalman filter.

Figure 5.8 gives details of the average flow simulated with the H-infinity filter on a monthly basis for a period from 1972 to 1980 for which the Sacramento model is calibrated. Here the model responded very well for every month.

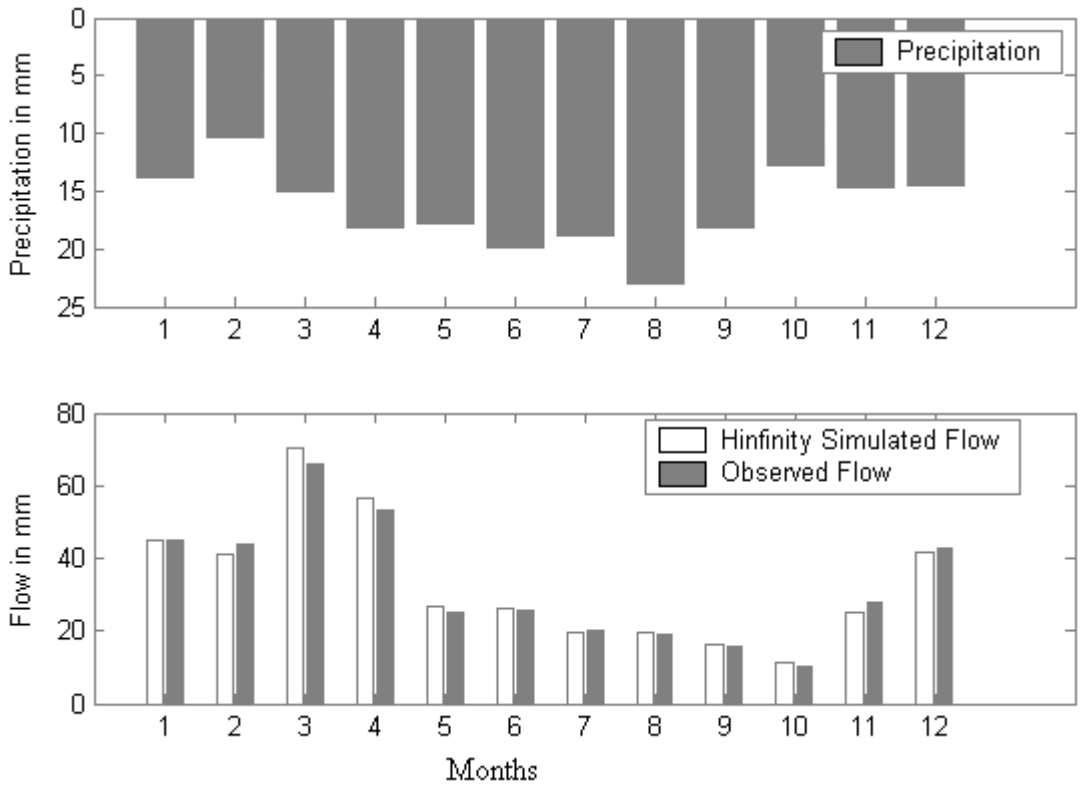

Figure 5.8: Average monthly flow for period from 1972 to 1980 when simulated by H-infinity filter.

Figure 5.9 gives details of the average flow simulated with the Kalman filter on a monthly basis for the calibration period from 1972 to 1980 is calibrated. Here the model responded very well. Comparing both the plots in Figure 5.8 and Figure 5.9, it can be observed that the H-infinity filter had better response than the Kalman filter in this period.

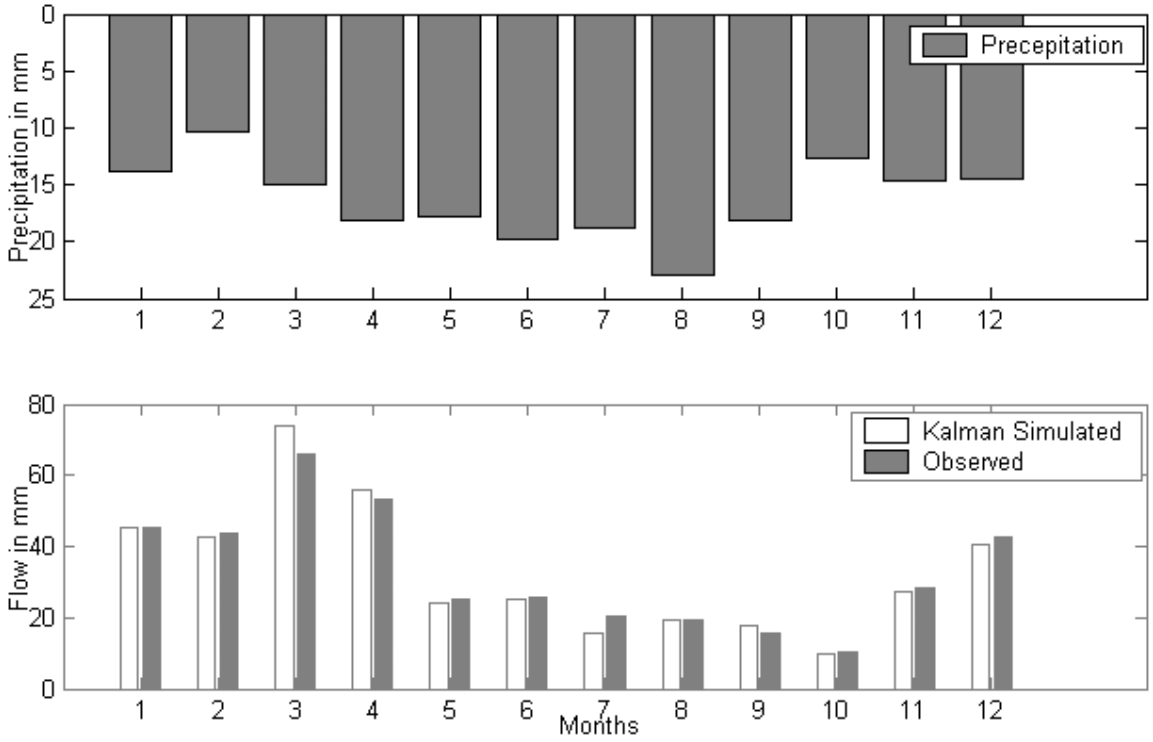

Figure 5.9: Average monthly flow for period from 1972 to 1980 when simulated by Kalman filter.

The filters here were tuned manually and heuristically. That is, the qualitative match between filter-predicted and measured streamflow was used as the criterion for tuning. Tuning of the filters is done to improve summery of performance measures. Here it can be observed that the Kalman filter is not able to respond for the sudden input changes, after a prolonged dry season as seen in Figure 5.1 and Figure 5.2. This may be because of the long memory that the Kalman filter is maintaining. H-infinity filter is called the minimax filter, where it minimizes the maximum errors. From the Figure 5.5, it can be observed that the H-infinity filter is tracking the output more efficiently than the Kalman filter. Here the calibrated Kalman filter is continuously under simulating the low flows, which corresponds to the more than half of days that are simulated. Moreover as these filters are manually tuned to get a good set of performance measures, there is still a possibility for tuning the filters better, so that they respond to all the changes in the input.

CHAPTER VI

CONCLUSION AND FUTURE WORK

The main aim of this thesis is to implement and evaluate optimal filtering techniques for a continuous hydrologic simulation model used for operational streamflow forecasting by the NWS and compare the results obtained from simulations. The Sacramento soil moisture accounting model is used by the National Weather Service to simulate and predict streamflow. The use of Kalman filtering in the field of streamflow forecasting [14] has been discussed for several decades, but it is not widely used and has largely been confined to research in the area. This thesis examines the implementation of the Kalman filter and the H-infinity filter in streamflow forecasting. This is the first time that H-infinity filtering has been used for streamflow forecasting. The results that are obtained, by calibrating the model for a period from 1972 to 1980, which is then tested for a period from 1967 to 1975, are summarized in Tables 6.1 and 6.2.

Model	E_{mean} =	$E_{persistence}$	Cumulative Water Error	Correlation	RMS
SS-SAC-SMA	0.73	0.48	20 mm	0.81	66.38
NWS simulated	0.75	0.57	60 mm	0.85	59.24
Kalman filter	0.78	0.63	17 mm	0.90	50.10
H-infinity Filter	0.81	0.67	40 mm	0.90	52.63

Table 6.1 Summary Table for calibration period from 1972 to 1980

Model	E_{mean}	$E_{persistence}$	Cumulative Water Error	Correlation	RMS
SS-SAC-SMA	0.67	0.53	461 mm	0.86	61.66
NWS simulated	0.70	0.67	380 mm	0.88	52.18
Kalman filter	0.78	0.35	–60 mm	0.79	49.66
H-infinity filter	0.87	0.65	44 mm	0.88	54.00

Table 6.2 Summary Table for testing period from 1967 to 1975

From the two tables it can be observed that the implementation of optimal filtering techniques for state estimation did improve the results, when it is compared with the NWS calibration of Sacramento soil moisture accounting model and the model without state updating. This helps in a good streamflow prediction. Moreover good streamflow prediction helps in forecasting floods and drought seasons ahead of time and precautionary measures can be taken considering the predictions. From the simulation the streamflow using the filters, each filter has its own advantage and disadvantage. While the streamflow simulated using H-infinity filter generated more runoff when there is little observed in the low flow period, the Kalman filter under simulated some of the peak flows

that occurred after prolonged dry season, and also it under simulated the low flow events. It is difficult to tell which filter is working better. As the filters are manually tuned to produce good results without exhibiting instability, filter performance may be improved by further tuning the filters. Tuning techniques like genetic algorithms [41], or Matlab's simplex functions [42], can be used to further improve the filter performance. Some work on calibration for the Sacramento model can be found in [47, 48, 49].

Here graphical comparison, Nash–Sutcliffe coefficient, correlation, water balance and the table of error comparison are used as performance measures of the simulation that is done. More performance measures can be used like peak and low flow criterion (PLC) [43], linear regression [44], goodness of fit and residual error analysis [44], which help us to identify the performance. More filtering methods can be used to estimate the states of the system like expert systems [45], neural networks [46], and combination of both the H-infinity and the Kalman filter.

The model is calibrated to the Deer Creek Watershed in Ohio. To check the working of the filter, this model can be calibrated and implemented in various watersheds in Ohio. Here optimal filtering techniques are implemented to estimate the states of the system.

BIBLIOGRAPHY

[1] Sherman, L.K, Streamflow from rainfall by a Unit Hydrograph Method, Eng. News Record, Vol. 108, pp. 501-505, 1932.

[2] Dooge, J.C. I., A General Theory of Unit Hydrograph, J. Geophysical Res., Vol. 64, No. 1, pp. 241, 1959.

[3] HEC, US Army Corps of Engineers, Hydrologic Eng. Center, HEC-1 Flood Hydrology Package, Programmers Manual, 1973.

[4] Metcalf and Eddy Inc., Storm Water Management Model, EPA report 110224DOC, 1971.

[5] Linsley, R.K. and Crawford, N.H, Computation of Synthetic Streamflow Record on Digital Computer, Hydrol. Sci. Bull. IASH, Pub. 51, pp. 526-538, 1960.

[6] Johanson, R.C. Imhoff, J.C., and Davis, H.H., Jr., User's Manual for the Hydrological Simulation Program-Fortran (HSPF), EPA Report FPA-600/9-80, 1980.

[7] NWS, National Weather Service River Forecast System Forecast Procedures, U.S. National Service Office of hydrology. NOAA Tech. Mem. NWS Hydro-14 Silver Spring, Md, 1972.

[8] Clarke, R.T, Mathematical Models in Hydrology, Irrigation and Drinage Paper No. 19, Food and Agriculture Organization of the United Nations, Rome, 1973.

[9] Fleming, G., Computer Simulation Techniques in Hydrology, Elsevier, 1975.

[10] Linsley, R.K., Rainfall-Runoff Models – An overview, Edited by V.P.Singh, Proc. Int. Symp. On Rainfall-Runoff Modeling, Mississippi State Univ., 1982.

[11] Veissman, W., Jr., et al., Introduction to Hydrology, 2nd Edition, 1972.

[12] Deg Hyo Bae and Konstantine P. Georgakakos, Hydrologic Modeling for Flow Forecasting and Climate Studies In Large Drainage Basins, University of Iowa, IIHR Report No. 360, 1992.

[13] Kitanidis, P.K and Bras, R.L, Adaptive Filtering Through Detection of Isoltaed Transient Errors in Rainfall-Runoff Models, in WRR Vol. 16, No. 4, pp. 740-748, 1980

[14] Kitanidis, P.K and Bras, R.L, Real-Time Forecasting With a Conceptual Hydrologic Model 1. Analysis of Uncertainty, WRR Vol. 16, No. 4, pp. 1025-1033, Dec.1980.

[15] Kitanidis, P.K and Bras, R.L, Real-Time Forecasting With a Conceptual Hydrologic Model 2. Applications and Results, WRR Vol. 16, No. 4, pp.1034-1044, 1980.

[16] J. Burl, Linear Optimal Control, Addison Wesley, 1999.

[17] Dr. Michael Ritter's website, University of Wisconsin web site, http//www.uwsp.edu/geo/faculty/ritter/geog101/uwsp_lectures/lecture_atmospheric_moisture.html

[18] NOAA's National Weather Service Regional Office Web Site, http://www.crh.noaa.gov/

[19] Burnash, R.J.C., Ferral, R.L. and Mcguire, R.A., "Generalized Streamflow Simulation System – Conceptual Modeling for Digital Computers," Technical Report, 204 pages (NWS), 1973.

[20] Puente C.E., Bras, R.L., Application of Nonlinear Filtering in Real-Time Forecasting of River Flow, WRR Vol. 23, No.4, pp. 675-682, 1987.

[21] Anderson, E.A, National Weather Service River Flow Forecast System – Snow Accumilation and Ablation Model, 1973.

[22] Willen, D.W., Shumway, C.A. and Reid, J.E., Simulation of Daily Snow Water Equivalent and Melt, Proceedings of Western Snow Conference, 1971.

[23] Y. H. Lee, and V. P. Singh, "Application of the Kalman filter to the Nash model," Hydrological Processes, Vol. 12, No. 5, pp. 755–767, 1998.

[24] Henrik Madesen, Automatic Calibration and Uncertainty Assessment in Rainfall-Runoff Modeling, DHI Water & Environment. Denmark.

[25] Dr. Georgakakos, Calibration of the Sacramento Soil Moisture Accounting Model, Demonstration of an Interactive Calibration Approach (Training Videos).

[26] Georgakakos, K.P., Bras, R.L, Real-time, Statistically Linearized, Adaptative Flood Routing, Water Resour. Res. Vol. 18, No. 3, pp. 513–524, 1982.

[27] Houser, P.R., Shuttleworth, W.J., Famiglietti, J.S., Gupta, H.V., Syed, K.R., Goodrich, D.C., 1998, Integration of Soil Moisture Remote Sensing and Hydrologic Modeling using Data Assimilation, Water Resour. Res. Vol. 34, No. 12, pp. 3405–3420.

[28] Li, J., Islam, S., On The Estimation of Soil Moisture Profile and Surface Fluxes Partitioning from Sequential Assimilation of Surface Layer Soil Moisture. J. Hydrol., Vol. 220, pp. 86–103, 1999.

[29] Kalman, R.E, A New Approach to Linear Filtering and Prediction Problems. J. Basic Engng., Vol. 82D, pp. 35–45, 1960.

[30] Refsgaard, J.C., Validation and Intercomparison of Different Updating Procedures for Real-Time Forecasting. Nordic Hydrol. Vol. 28, pp. 65–84, 1997.

[31] Tamer Basar and Pierre Bernhard, H-infinity Optimal Control and Related Minimax Design Problems. Second Edition Birkhäuser, Boston, 1995.

[32] Arthur Gelb, Applied Optimal Estimation, The M.I.T press, 1974.

[33] D. Simon and H. El-Sherief, Hybrid Kalman / Minimax Filtering in Phase-Locked Loops, Control Engineering Practice, Vol. 4, pp. 615-623, October 1996.

[34] Mohinder S. Grewal and Angus P. Andrews, Kalman Filtering Theory and Practice Using Matlab, John Wily & Sons, 2001.

[35] Pavel Chigansky, On Exponential Stability of Nonlinear Filtering for Slowly Switching Markov Chains, Arxiv preprint math, arxiv.org, PR/0411596, 2004

[36] R. Atar, O. Zeitouni, Lyapunov Exponents for Finite State Nonlinear Filtering. SIAM J. Control Optim, Vol. 35, No. 1, 36–55, 1997.

[37] David Aubert, Ce´cile Loumagne, Ludovic Oudin, Sequential Assimilation of Soil Moisture and Streamflow Data in a Conceptual Rainfall–Runoff Model, Journal of Hydrology, Vol. 280, No. 1, pp. 145-161(17), September 2003.

[38] Konrad Reif, Stefan Gunther, Engin Yaz, and Rolf Unbehauen, Stochastic Stability of the Discrete-Time Extended Kalman Filter, IEEE Transactions on Automatic Control, Vol. 44, No. 4, pp. 714-728, April 1999.

[39] Nash, J.E., Sutcliffe, J.V, River Flow Forecasting through Conceptual Model Part I-A Discussion of Principles. Journal of Hydrology, Vol. 10, pp. 282-290, 1970.

[40] Grunwald, S., and Frede, H.-G., Using the Modified Agricultural Non-point Source Pollution Model in German Watershed. Catena, Vol 37, pp. 319-328, 1999.

[41] M. Mitchell, An Introduction to Genetic Algorithms, The MIT Press, 1996.

[42] J. A. Nelder and R. Mead, A Simplex Method for Function Minimization, Computer Journal, Vol. 7, pp. 308-313.

[43] Paulin Coulibaly, Bernard Bob and Francois Anctil, Improving Extreme Hydrologic Events Forecasting Using a New Criterion for Artificial Neural Network Selection, Hydrological process, Scientific briefing , Hydrol. Process. Vol. 15, pp. 1533–1536, 2001.

[44] Mulla, D.J., and T.M. Addiscott, Validation approaches for field-, basin-, and regional-scale water quality models. In: D.L. Corwin, K. Loague, and T.R. Elsworth (eds) Assessment of Non-Point Source Pollution in the Vadose Zone, Geophysical Monogroaph 108, American Geophysical Union, Washington, D.C, pp. 63-78, 1999.

[45] H. DePold and F. Gass, The Application of Expert Systems and Neural Networks to Gas Turbine Prognostics and Diagnostics," ASME Journal of Engineering for Gas Turbines and Power, Vol. 232, pp. 607-61, Oct. 1999.

[46] Hjelmfelt, A. T. and M. Wang, "Predicting Runoff Using Artificial Neural Networks," Surface Water Hydrology, pp. 233-244, 1996.

[47] Q. Duan, S. Sorooshian, and V. Gupta "Effective and Efficient Global Optimization for Conceptual Rainfall-Runoff Models", Water Resources Research, Vol 28, No. 4, pp.1015-1031, 1992.

[48] Q. Duan, V.K. Gupta and S. Sorooshian, A Shuffled Complex Evolution Approach for Effective and Efficient Global Minimization, Journal of Optimization Theory and its Applications, Vol. 76, No. 3, pp. 501-521, 1993.

[49] Q. Duan, S. Sorooshian, & V.K. Gupta, Optimal Use of the SCE-UA Global Optimization Method for Calibrating Watershed Models, Journal of Hydrology, Vol.158, pp. 265-284, 1994.

[50] Arthur J Krener, The Convergence of the Extended Kalman Filter, in Directions in Mathematical Systems Theory and Optimization, A. Rantzer and C. I. Byrnes, eds., Springer Verlag, Berlin, pp.173-182, 2002.